First Wall Protection in ICF Reactors by Inert Cavity Gases

G.A. Moses and R.R. Peterson

October 1979

UWFDM-323

FUSION TECHNOLOGY INSTITUTE

UNIVERSITY OF WISCONSIN

MADISON WISCONSIN

First Wall Protection in ICF Reactors by Inert Cavity Gases

G.A. Moses and R.R. Peterson

Fusion Technology Institute
University of Wisconsin
1500 Engineering Drive
Madison, WI 53706

http://fti.neep.wisc.edu

October 1979

UWFDM-323

First Wall Protection in ICF Reactors by Inert Cavity Gases

Gregory A. Moses
Robert R. Peterson

October 1979

UWFDM-323

Fusion Engineering Program
Nuclear Engineering Department
University of Wisconsin
Madison, Wisconsin 53706

This work was supported by Sandia Laboratory under Contract #DSG/06-9329.
Submitted for publication to Nuclear Fusion.

I. Introduction

The inertial confinement approach to controlled thermonuclear fusion involves the compression of the fusion fuel to densities of 1000 times normal liquid density.[1,2] At these high densities, the inertia of the fuel itself and other surrounding tamper material is great enough to hold the fuel together for a time that is longer than the characteristic thermonuclear burn time. If this compression of the fuel is produced in an efficient way, then a net energy gain will result. The compression of the fuel is accomplished by the implosion of spherical fusion pellets by an energy source of high intensity. A variety of different "drivers" have been proposed for the purposes of providing this energy. These include lasers, relativistic electron beams, light ion beams, and heavy ion beams. In each case the beam energy from the driver ablates the outer part of the fusion pellet, creating a force that spherically implodes the inner fuel part of the pellet to thermonuclear ignition conditions. Also, in each case, once the pellet has ignited and burned, it is left in a very explosive condition. About 20%-30% of the fusion energy from the DT reaction is left behind in the pellet. The remainder escapes in the form of 14.1 MeV neutrons. For a pellet energy gain of 100 there is 20-30 times as much internal energy in the pellet following the burn as there was before burning started. Following the thermonuclear burning the pellet violently explodes creating high energy ion debris and X-rays.[3]

These ion debris and X-rays pose serious problems for inertial confinement fusion reactors.[4,5] The ions and X-rays have short mean free paths in solid materials and therefore act as a surface heat source to the reactor first wall.

Furthermore, this heat flux is pulsed and can attain very high instantaneous values. As a result of this problem, the study of inertial confinement fusion (ICF) reactor design has concentrated to a large extent on methods to protect the first wall from this transient surface heat load. In fact the distinguishing feature in each different design is always the first wall protection mechanism. Among the schemes that have been proposed are: the lithium wetted wall[6], the magnetically protected wall[7], the liquid lithium "waterfall" or jets[8,9], and the gas filled cavity[10-13]. In this paper we report an analysis of the gas filled cavity concept for ICF reactor first wall protection. This concept has potential application in at least two forms of ICF, laser fusion and light ion beam fusion.

For laser fusion reactors this concept was proposed in the SOLASE[10-12] design of the University of Wisconsin. In this design a 6 m radius spherical cavity is filled with 0.25-0.5 torr of a noble gas, such as Ne or Xe. The choice of a noble gas is motivated by fears of laser induced gas breakdown as the beams pass through the gas to the target. The first wall in the reactor is graphite. Calculations show that this amount of gas will attenuate the target X-rays and thermalize the ion debris from a representative exploding target before they reach the first wall. It is then postulated that the energy deposited in the gas will be re-radiated to the first wall in a pulse of greater than a millisecond in duration. Such a long pulse can be thermally accommodated by the graphite wall. This behavior is crucial to the feasibility of gas protection in laser fusion reactors as conceived in the SOLASE concept. The gas must act as a "thermal capacitor" to transform heat pulses of nanosecond duration into heat pulses of millisecond duration.

Gas protection of the first wall in a light ion beam fusion reactor[13] comes as a natural consequence of the means to propagate the ion beams from their diodes to the target. In this fusion concept it is proposed to break down ionized channels in a background gas to serve as "renewable electrical connections" between the individual diodes and the target.[14] To meet this need it is estimated that 10-100 torr of gas is required. This is a considerably higher pressure than in the laser fusion case. Therefore, in a light ion beam (LIB) fusion reactor the first wall will be automatically protected from the exploding target. In this high pressure cavity and the low pressure cavity of laser fusion it is essential to understand the behavior of this gas, once the pellet debris has been deposited into it. It must be verified that the gas will actually serve as a thermal capacitor, and if it does, then the detailed dynamics of the gas must be known to design the first wall.

In this paper we report the development of a new computer code to model the response of the cavity gases to the sudden introduction of energy by the exploding pellet. This code is utilized to predict the response of both high pressure (LIB reactors) and low pressure (laser reactors) cavity gases. Particular attention is paid to the behavior of noble gases, but non-noble gas behavior is also included for comparison purposes. Numerous calculations are presented for varying combinations of important parameters so that a catalog of results as a function of these parameters can be assembled. In addition, a detailed look at the basic phenomena that control the gas response in the high and low pressure cases is given. This is necessary because several heretofore unpredicted or unrecognized phenomena are shown to be very important to the gas dynamics. Part II of this paper is a discussion of the high pressure gas filled cavity with applications to LIB fusion and Part III is a similar discussion of the low pressure gas that

is associated with laser fusion. Because the results of each of these cases are quite different, the conclusions and implications of the results are discussed at the end of each part rather than in combination at the end of the paper.

II. High Pressure Cavity Gas - Light Ion Beam Applications

Phenomenology

The cavity gas pressure for light ion beam reactors is estimated to be from 10-100 torr when measured at 0°C. The actual property of importance is the gas number density and this is 3.5×10^{17} to $3.5 \times 10^{18} cm^{-3}$ at this pressure and temperature. The cavity gas temperature will certainly not be 0°C and thus the pressure will be higher than 10-100 torr. However, a convention in this field has been established that the gas density is given in terms of its pressure at 0°C. This convention will be used in all of the following discussions except where specifically noted. This gas density is required to provide a sufficient electron density in the ionized channel that is established between the diode and the target. This is related to the return current that is necessary for current neutralization as the light ion beam propagates down the channel. A detailed discussion of this problem is not important to the considerations in this paper. The major point to be made here is that this gas density will very effectively attenuate the X-ray energy and thermalize the ions that result from the target explosion. For light ion beam targets the X-ray spectrum will have an effective temperature less than 1 keV. Such a blackbody spectrum will be absorbed within 10 cm of the target. Likewise, the ion debris spectra will be soft due to the high Z material in the pellet. It is therefore postulated that the pellet explosion will almost instantaneously put the cavity gas in an initial state characterized by a hot ball of plasma with a radius of ~10 cm at the center of the cavity, surrounded by cold gas out to the first wall. This is the model that is used for all of the high pressure gas calculations.

This model is certainly an idealization of the actual dynamics of the pellet exploding into the gas immediately surrounding it. However, since we expect that the propagation of the pellet energy obeys something resembling strong shock theory[15], the only important initial parameters should be the energy and the mass density. Work is currently underway to study this problem in more detail, but for our analysis the effect of this idealization will only be tested parametrically.

The hot ball of plasma created by the pellet explosion is called a fireball. Fireballs have been studied extensively as part of the nuclear weapons atmospheric testing program[16]. The behavior of fireballs can be described using Fig. 1. The two major ingredients of a fireball are plasma and the radiation field associated with this plasma. Figure 2 shows the energy density of argon plasma at densities of $1.67 \times 10^{18} cm^{-3}$ and $6.0 \times 10^{17} cm^{-3}$ as a function of temperature. Included on this same graph is a plot of the equilibrium radiation energy density that is associated with these plasmas. Both densities are considered because for a gas initially at $1.67 \times 10^{18} cm^{-3}$, the density inside the fireball quickly drops to $6 \times 10^{17} cm^{-3}$. Note that above a temperature of 80 eV the majority of the total energy in the fireball is in the form of radiation. Since radiative energy is more easily transported, it is therefore not surprising that the behavior of this radiation plays a very important role in the fireball dynamics. Figure 1 shows the state of the fireball at three important times in its evolution. Initially the fireball is a hot plasma with its radiation in equilibrium at a temperature T, greater than the transparency temperature

of the plasma. Hence the radiation mean free path is short and all of the fireball energy is "trapped" behind a spherical front that is being pushed outward by the difference in pressure ahead and behind it. This phenomenon is often described by strong shock theory,[15] which predicts that the shock velocity is given by the expression

$$\dot{R}(t) = \frac{2}{3}\,\xi_o\left(\frac{E_{in}}{\rho_o}\right)^{1/5} t^{-3/5} \quad ,$$

where E_{in} is the initial fireball energy, ρ_o is the initial gas density, and ξ_o is a constant dependent upon the gas. This will be the case so long as the fireball energy is trapped behind the shock and the pressure ratio behind and ahead of the shock is large (~10). As the shock expands outward, the temperature of the plasma behind it drops until the transparency temperature is reached. This is the temperature at which the plasma becomes transparent to the radiation that was previously in equilibrium with it. The radiation mean free path becomes large in comparison to the fireball dimensions. At this point the radiation "leaks" through the shock front and the temperature of the fireball falls more quickly than before. At this point, a free shock is launched with the temperature and pressure profiles decoupling as shown in Fig. 1-b. This shock then propagates to the first wall.

Computer Model

The phenomena described above are the result of a complex synergism between radiative processes and hydrodynamics. To more fully understand this complex process a computer model has been developed to include the essential features of the fireball dynamics. The computer code has been given the name FIRE. In the FIRE code, the plasma/gas motion is described in the one

fluid hydrodynamic approximation. The equation of motion is expressed in lagrangian coordinates as

$$\frac{\partial u}{\partial t} = -x^{\delta-1} \frac{\partial}{\partial m_o} (P+Q) \tag{1}$$

where m_o is the lagrangian variable defined as

$$dm_o = x^{\delta-1}\rho(x)dx. \tag{2}$$

The other quantities are the fluid velocity u, the total pressure P, the mass density ρ, and one spatial dimension x (δ=1 planar, δ=2 cylindrical, δ=3 spherical). The standard shock treatment using a Von Neumann artificial viscosity Q is used.[17] This spreads the shock front over about 3 finite difference zones while preserving the Heugoniot relations across the shock. This equation is solved for the fluid velocity using an explicit differencing technique which, for numerical stability, requires the satisfaction of the Courant condition[18]

$$\Delta t < \Delta x/C_s \tag{3}$$

where Δt is the time step, Δx is a finite difference zone width and C_s is the local sound speed. This limits the time step so that disturbances cannot propagate across a zone in less than one time step. The plasma is characterized by a local temperature $T_p(x,t)$. Thermal energy flow through the plasma includes electron thermal conduction and radiation transport. Radiation transport is treated by modelling the radiation field as a fluid with its own local temperature, $T_r(x,t)$.[19] This temperature can be different from the plasma temperature. Two coupled diffusion equations are then solved for the thermal transport in the plasma. These are

$$C_{vp} \frac{\partial T_p}{\partial t} = \frac{\partial}{\partial m_o} (x^{\delta-1} K_p \frac{\partial T_p}{dx}) - w_{pr}(T_p-T_r)-(P_p)_T \frac{\partial V}{\partial t} T_p \tag{4}$$

and

$$C_{vr} \frac{\partial T_r}{\partial t} = \frac{\partial}{\partial m_o} (x^{\delta-1} K_r \frac{\partial T_r}{\partial x}) + w_{pr}(T_p-T_r) - (P_r)_T \frac{\partial V}{\partial t} T_r. \tag{5}$$

where C_{vp} and C_{vr} are the specific heats at constant volume for the plasma and radiation, K_p[22] and K_r[19] are the thermal conductivities for the plasma and radiation, $(P_p)_T$ and $(P_r)_T$ are the temperature derivatives of the plasma and radiation pressures, and V is the plasma specific volume. The emission and absorption of radiation is treated by the coupling term $w_{pr}(T_r-T_p)$. For the calculation presented in this paper, the radiative transfer of energy is the most dominant effect. The two equations are solved simultaneously using a fully implicit finite difference technique.[21,22] Two "adjustments" must be added to the solution of these non-linear diffusion equations to insure physical relevance and numerical stability. First, the radiation diffusion equation is flux limited. The flux across a zone boundary is not allowed to exceed cE_r, which is the free streaming limit of radiation flux in a vacuum. This allows the diffusion model to be used in non-diffusive problems while continuing to provide physically plausible results. Second, upstream averaging is used to evaluate the radiation properties near the edge of the fireball. This allows radiation to flow from a hot zone where its heat capacity, $C_{vr} \sim T^3$, is high to a cold zone where its heat capacity is low without resorting to diminishingly small times to control accuracy. This also avoids bothersome numerical instabilities that result from this non-linear problem. The two-temperature approximation allows the radiation to come into equilibrium at whatever temperature that it wishes. This is shown schematically in Fig. 1a where the cold plasma is transparent to the radiation but the plasma at the edge of the fireball is not. Hence the radiation is the region between the fireball and the wall is in equilibrium with the hot plasma at the edge of the fireball while the plasma temperature between the fireball and the wall remains low. This is shown to be crucial to the results of fireball dynamics in noble gases. One temperature models[23], such as used in the CHART-D code, may not accurately treat

this phenomenon. Codes using multi-frequency radiation diffusion would of course offer a better model but these are much more expensive to use. The two temperature model used here is a good compromise.

A most important feature of this model is the equation of state and radiative property data. In fact, the behavior of these quantities in the non-linear coefficients of the hydrodynamics equations is the key to the results obtained in this paper. For the FIRE code, these data are stored in tabulated form as a function of density, plasma temperature, and radiation temperature. The tabulated quantities include: plasma specific internal energy $E(\rho,T_p)$, plasma average charge state $\bar{Z}(\rho,T_p)$, Planck averaged radiation mean free path $\ell_1(\rho,T_p,T_r)$, and Rosseland averaged radiation mean free path $\ell(\rho,T_p,T_r)$. These quantities are computed using a semi-classical model of the atom[24] using another computer code named MFP.[25] The Planck averaged mean free path is shown in Fig. 3 as a function of the plasma and radiation temperatures for a fixed argon plasma density.

For most of the calculations that follow the spherical cavity gas volume is divided into 50 spatial zones and 14,000 time steps are used to span 3-5 ms of physical time. These calculations require 3 ms/zone·cycle on a UNIVAC 1110 computer. This represents a modest cost for the computations.

Calculational Results

In the results that follow, it is assumed that the pellet X-ray and debris energy is stopped in the first 10 cm surrounding the pellet. This is the size of the initial fireball, at t = 0. The pellet mass is taken to be additional cavity gas mass (only one ion specie is allowed in the FIRE code) and is uniformly distributed in the 10 cm initial fireball. Equal mass zoning is used at the center of the gas volume (10 zones), near the initial

fireball, and also near the first wall (10 zones). This gives the most accurate treatment of the gas motion. In between (30 zones) there is a smooth variation in zone mass to avoid "numerical reflections" of lighter zones from heavier ones.

The details of a representative calculation are given in Table 1. The 30 MJ of yield that is deposited in the gas would correspond to a total yield of 100-150 MJ when the 14.1 MeV neutrons are included. This is a range of yield that is considered for light ion beam driven targets.[26,27] The general features of fireball dynamics that are described in the earlier section on phenomenology are numerically verified in this example. Figure 4 is a plot of the plasma temperature profiles in the plasma as a function of radius at different times during the shock propagation to the wall. Figure 5 is a similar plot of the pressure. Figure 6 is a plot of the heat flux and mechanical overpressure experienced at the first wall as a function of time and Fig. 7 is a plot of the Planck and Rosseland averaged radiation mean free paths as functions of the plasma and radiation temperatures when they are equal. Figure 7 shows that the argon plasma becomes transparent to its equilibrium radiation at a temperature of ~1 eV. Figure 4 shows that the fireball reaches this temperature at a time between 0.1 ms and 0.46 ms after the fireball creation and Fig. 6 indicates that this is when the first wall experiences the heat flux leaking from the fireball. Figures 4 and 5 show that the shock has separated from the fireball by 0.46 ms and propagates to the wall by itself. Figure 8 is an R-t plot of the gas motion. Each line in this plot follows the trajectory of a unit of mass as a function of time. The shock can be clearly seen as a bunching of the lines. The prediction of

Table 1

Input Parameters for FIRE Calculations

Cavity radius (m)	4	4
Gas type	Argon	Diatomic Ar
Gas pressure at 0°C (torr)	50	50
Gas number density (cm^{-3})	1.67×10^{18}	1.67×10^{18}
Gas mass density (g/cm^3)	1.114×10^{-4}	1.114×10^{-4}
Energy deposited in fireball (MJ)	30	30
Initial fireball radius (cm)	10	10
Initial fireball temperature (eV)	64	64
Initial fireball charge state	12	12
Maximum overpressure (atm)	1.5	2.75
Time of maximum overpressure (ms)	2.3	1.7
Energy radiated to wall (MJ)	7.5	0.15
Average heat flux* (kW/cm^2)	15	0.05
Pulse width* (μs)	110	1500

*The average heat flux is defined as the energy radiated to the first wall divided by the pulse width.

strong shock theory is also plotted on Fig. 8 and we see that the shock speed begins to deviate from strong shock theory early in time. The heat flux at the wall averaged over the pulse width is 15 kW/cm^2. This is unacceptably large for reactor applications. The resultant temperature rise in a 0.5 cm stainless steel wall is 317°C when the repetition rate is 10 Hz.

All of these results are attributable to the high transparency temperature of argon, Fig. 7. Air, for instance, has a transparency temperature of 0.2 eV. The high transparency of argon at temperatures below 1 eV is due to the monatomic nature of the molecule. Electronic transitions are the lowest transitions available to strongly absorb a photon. Hence, photons below about 16 eV are only weakly absorbed. This situation is much different for polyatomic molecules where the rotational and vibrational transitions are available to absorb low energy photons. Hence the transparency temperature of these gases is much lower. To demonstrate the importance of this point, the argon data used in the example calculation is modified so that the radiation mean free path path below 1.5 eV is limited to no greater than 50 cm. This gas we call "diatomic argon". The results of an identical calculation using this gas are also given in Table 1 and are displayed in Fig. 9. From Fig. 9 we see that the heat flux comes only after the pressure pulse has hit the first wall and the maximum heat flux is only 0.13 kW/cm^2. On the other hand, the overpressure is greater in this case because energy is never leaked from the fireball before the shock arrives at the wall. This comparison verifies the assertion that the high transparency of noble gases at low temperature leads to the premature release of the radiant energy in the fireball. Therefore, a strong distinction exists between the behavior of noble and non-noble gases in high pressure reactor cavities.

A variety of other calculations have been done to determine the effect of changing various important parameters. In Table 2 the tabulated results of calculations using different initial argon temperatures are given. In each case a 30 MJ fireball is started in the center 10 cm of the cavity. These different initial temperatures correspond to different mass flow rates of argon through the cavity for a system in cyclic steady state. The total radiant energy transferred to the first wall increases with increasing temperature. This is because the gas surrounding the fireball has an increasing amount of energy associated with it as its temperature increases. At a temperature of 1.0 eV for instance, there is more energy radiated to the first wall than is in the fireball. This is clearly a non-physical result. The point to be made here is that at a gas temperature between 0.7 and 1.0 eV (actually ~0.73 eV) the gas will radiate 30 MJ to the wall for every 30 MJ deposited into in at a repetition rate of 1 to 10 HZ. At this equilibrium point, no gas circulation through the cavity is needed to maintain cyclic steady-state operation at this temperature. To maintain cyclic steady state temperatures below 0.73 eV the gas must be circulated through an external heat exchanger. The mass flow rates are given for a 1 Hz repetition rate. The results of using xenon rather than argon as the cavity gas are given in Table 3. From this result, it is seen that for identical initial conditions, xenon gas allows a much lower amount of radiant heat to reach the first wall than argon gas. This occurs because the heat capacity of xenon is larger than that of argon so that 30 MJ of energy raises the gas to a lower temperature where a smaller percent of the energy is in radiation. With less radiant energy in the system, the heat fluxes should be lower. Also, the radiation mean free paths tend to be shorter for xenon than for argon. Even though there is less energy lost via radiation, the overpressure at the wall is no larger. The scaling of the results with target yield are also demonstrated

Table 2

Wall Overpressures and Radiant Heat Fluxes for Argon Cavity Gas at Different Temperatures

E_{in} = 30 MJ		$N_p = 1.67 \times 10^{18} cm^{-3}$			R_{wall} = 4 m
T_{pcav} (eV)	$P_{wall-max}$ (atm)	$P_{initial}$ (atm)	ΔP (atm)	E_{out} (MJ)	$\langle \underline{q} \rangle''_{pulse}$* ($kW/cm^2$)
0.05	1.3	.113	1.17	6.6	21.9
0.1	1.5	.275	1.23	7.5	15.0
0.5	2.5	1.33	1.17	14.7	24.5
0.7	2.75	1.98	.78	20.3	29.2
1.0	3.0	2.95	.05	148	52.6

*$\langle \underline{q} \rangle''_{pulse}$ is defined as the energy radiated to the first wall divided by the pulse width.

Table 3

Comparison of High Pressure Blast Waves

$N_p = 1.67 \times 10^{18} cm^{-3}$		$T_{pcav} = .1$ eV	
GAS SPECIES	ARGON	XENON	ARGON
E_{in} (MJ)	30	30	100
$P_{wall-max}$(atm)	1.5	1.5	4.26
P_{init} (atm)	.27	.26	.27
ΔP_{wall} (atm)	1.23	1.25	4.0
E_{out} (MJ)	7.5	3.5	17.1
$\langle \underline{q} \rangle''_{pulse} (\frac{kW}{cm^2})$ *	15	7.9	21.3
$\dot{m}$(gm/sec)	3.3×10^4	9.7×10^4	1.3×10^5

*$\langle \underline{q} \rangle''_{pulse}$ is defined as the energy radiated to the first wall divided by the pulse width.

in Table 3 where the 30 MJ shot in argon is compared to a 100 MJ shot. The 100 MJ shot would correspond to a total yield of 333-500 MJ. The average heat flux at the wall is not substantially greater for the 100 MJ fireball, but the maximum overpressure is nearly 3 times as large. This latter point indicates that although the absolute value of the overpressure is not well predicted by strong shock theory, the relative magnitudes scale linearly with the explosion energy as would be predicted by strong shock theory.

Conclusions of High Pressure Results

(1) The strong shock theory of Taylor[15] does not adequately treat the propagation of a fireball through typical light ion beam fusion reactor cavity gases. (2) The gas temperature and pressure profiles indicate that the shock wave separates from the fireball long before it reaches the wall of a 4m radius cavity. (3) Radiant heat fluxes measured at the first wall are large for argon gas at a pressure of 50 torr. These lead to high temperature transients in a stainless steel wall. (4) This large (~20 kW/cm^2) instantaneous heat flux is the result of an unusually high transparency temperature for noble gases. This allows the radiation to "leak"from the fireball while it is still very hot. (5) Diatomic gases may be better suited than noble gases for the cavity gas in light ion beam fusion reactors because they will not become as transparent and volumetrically radiate their energy to the first wall at high temperatures (~1 eV). (6) The heat flux experienced by the first wall for non-noble gases is very low although the maximum overpressure is greater. However, mechanical design studies[28] show that this mechanical overpressure can be easily accommodated using standard engineering design techniques, and stainless steel as the first wall material. (7) On the other hand, if a large heat flux can be tolerated, as in a "single shot facility" or a materials test facility with a low duty cycle, then noble gases offer the opportunity to reduce the overpressure created by the blast wave. (8) Heavier noble gases, such as xenon, have larger heat capacities and shorter radiation mean free paths and will be more effective than argon in protecting the first wall from large radiant heat fluxes.

(9) In general, gas protection of the first wall in LIB fusion reactors is substantiated by these results. The gas type and temperature can be tailored to meet a whole range of specific requirements.

III. Low Pressure Cavity Gas - Laser Fusion Applications

Phenomenology

The gas pressure in a laser fusion reactor cavity must satisfy two conflicting criteria. The gas density must be low enough to insure that the laser beams will not be steered from the target by laser induced gas breakdown. On the other hand, the gas density must be sufficiently high to stop the charged particle debris and X-rays from the exploding pellet before they reach the wall. Unfortunately, the first of these limits is unknown and the second depends on the output spectra of the target which is also not well established.

Theoretical estimates show that laser induced gas breakdown will occur at pressures of 0.1 to 1 torr for noble gases and laser intensities on the order of those required for laser fusion.[10-12] Noble gases are thought to be particularly important to laser fusion applications because they possess a high ionization potential compared to non-noble gases. This presumably increases the breakdown threshold intensity of the laser light. However, the theories of breakdown do not accurately describe the results of many experiments and the viability of cavity gases in laser fusion reactors still must be determined by experiment. For the purposes of this study we assume that pellets can be successfully irradiated in 0.25 torr of a noble gas such as Ar or Xe.

Calculations also indicate that 0.1-1.0 torr of xenon gas will stop the ion debris and X-rays for a representative pellet output spectra.[29] For this low pressure gas and the representative pellet spectra, the output energy will not be stopped in a small volume surrounding the pellet but will be distributed through the gas in some profile that may extend to the first wall.

The gas response to this deposited energy is very important because it must hold this energy and re-radiate it to the first wall in a long pulse (~msec). This is the key element of the gas protection scheme proposed in the SOLASE laser fusion reactor study.

Computer Model

The computer model used for these calculations is the same one described in Part II. We should note that the low pressure gas calculations extend this model to its limit of validity because much of the phenomena that are predicted are non-diffusive in nature. This means that the model is operating in the flux limited mode for much of the calculation. However, the physical plausibility of the results will be stressed where appropriate.

Computational Results

In the following calculations, equal radii zoning is used rather than equal mass zoning. This makes very little difference in these computations because there is almost no motion of the gas.

In Table 6 we present the results of a calculation for 0.25 torr of xenon in a 6 meter cavity with a deposited energy of 30 MJ. This energy is assumed to be uniformly deposited in a 1 meter sphere surrounding the pellet. These results might be considered to correspond to the SOLASE reactor cavity situation. The heat flux and overpressure experienced at the first wall are shown in Fig. 10. The average heat flux, computed as the energy radiated to the wall in the high intensity part of the pulse divided by the width of this pulse, is 40.2 kW/cm^2. This heat flux is much higher than the estimate

Table 6

Fireball Calculation of 1/4 torr of Xenon in a 6 meter Cavity

Cavity Radius	6 meter
Gas Type	Xe
Gas Pressure (0°C)	0.25 torr
Energy Deposited	30 MJ
Initial Fireball Radius	1 meter
Initial Fireball Temperature	23.5 eV
Initial Gas Temperature	0.1 eV
Maximum Overpressure	13.7 torr
Time of Maximum Overpressure	23 μs
Energy Radiated to First Wall*	10 MJ
Average Heat Flux**	40.2 kW/cm^2
Pulse Width**	55 μs

* The energy radiated to the wall is defined as the amount of energy radiated for instantaneous values of the heat flux greater than 10% of the maximum.

** The average heat flux is defined as the energy radiated to the first wall divided by the pulse width.

used in the SOLASE study and leads to a temperature rise in the first wall of 1740°C. However, the overpressure experienced at the wall is very low, 14 torr. This is lower than the design value in SOLASE.

The reason for this very large heat flux can be learned from studying the plasma and radiation temperature profiles in the xenon gas along with the radiation mean free path. A snapshot plot of these is given in Fig. 11 at a time of 0.65 μs. This low pressure calculation is significantly different in character than the high pressure ones discussed in Part III of this paper. In this low pressure case the radiation mean free path in the hot fireball is very long and the mean free path in the surrounding cold gas is very long. However, in the temperature gradient between these two, there is a region of plasma where the mean free path is short. This is at a radius of about 400 cm in the snapshot shown in Fig. 11. This opaque region of plasma prevents the radiation behind it from streaming to the first wall. Note that the radiation temperature in the fireball has nearly come into equilibrium with this plasma region at a temperature of 2 eV, while the plasma temperature in the fireball is still 5-10 eV. This decoupling of the temperatures points out the importance of the two temperature model used in these calculations. This situation continues until this opaque plasma region has propagated to the first wall, at 2.8 μs. At this time the first wall is almost instantaneously exposed to all of the hot plasma behind this barrier; the fireball volumetrically radiates to the first wall. This results in a very large instantaneous heat flux. The heat flux decays very quickly because the fireball is rapidly losing energy and its temperature is dropping. Thus in this example the cavity gas very

effectively holds the explosion energy until the thermal wave created by the energy deposition reaches the first wall. Then the energy is rapidly radiated to the first wall.

The rather special set of circumstances that lead to this result cast doubt on the general applicability of this behavior over the range of uncertainties associated with the fireball creation process. The initial conditions are of course determined by the pellet output spectra. This problem is studied parametrically by assuming that the pellet energy is deposited in spheres of radii 1 meter, 3 meters, and 5 meters surrounding the pellet. The results of all of these calculations are presented in Table 7 for a 30 MJ charged particle and X-ray yield and 0.25 torr of xenon in a 6 meter cavity. As the initial fireball radius becomes larger, the amount of energy radiated to the wall increases but the time over which this energy is radiated also increases substantially. Hence the average heat flux incident on the wall decreases with increasing fireball radius. However, this heat flux is still substantial and the gas displays the same characteristics in all three cases. It only holds the deposited energy for about 0.1 msec whereas the graphite wall designs require a re-radiation time of greater than 1.0 msec.

A comparison of three different yield energies (10 MJ, 30 MJ, 100 MJ) is given in Table 8. These would roughly correspond to total pellet yields of 33, 100 and 330 MJ. The average heat flux increases dramatically from a 30 MJ to 100 MJ yield whereas the increase is only a factor of two between 10 MJ and 30 MJ yields. This can be explained by noting that the gas temperature rapidly drops to about 0.5-1.0 eV in all cases once the fireball reaches the wall. The energy radiated to the wall is then the difference

Table 7

Comparison of 1, 3, and 5 m Fireballs for a 30 MJ Fireball in 1/4 Torr of Xenon

	Fireball Radius		
	1 m	3 m	5 m
Cavity Radius (m)	6	6	6
Gas Type	Xe	Xe	Xe
Gas Pressure (0°C) (torr)	0.25	0.25	0.25
Energy Deposited (MJ)	30	30	30
Initial Fireball Temperature (eV)	23.5	4.5	2.0
Initial Gas Temperature (eV)	0.1	0.1	0.1
Maximum Overpressure (torr)	13.7	15.2	18.2
Time of Maximum Overpressure (μs)	23	25	1000
Energy Radiated to First Wall* (MJ)	10	14.5	14.7
Average Heat Flux** (kW/cm^2)	40.2	25.6	18.5
Pulse Width** (μs)	55	125	175

*The energy radiated to the first wall is defined as the amount of energy radiated for instantaneous values of the heat flux greater than 10% of the maximum.

**The average heat flux is defined as the energy radiated to the first wall divided by the pulse width.

Table 8

Comparison of Different Yields for 0.25 Torr Xenon in a 6 m Cavity

	Energy Deposited (MJ)		
	10	30	100
Cavity Radius (m)	6	6	6
Gas Type	Xe	Xe	Xe
Gas Pressure (0°C) (torr)	0.25	0.25	0.25
Initial Fireball Radius (m)	1	1	1
Initial Fireball Temperature (eV)	14	23.5	35
Initial Gas Temperature (eV)	0.1	0.1	0.1
Maximum Overpressure (torr)	2.4×10^{-3}	13.7	83.6
Time of Maximum Overpressure (μs)	1000	23	1.8
Energy Radiated to First Wall* (MJ)	2.0	10	53
Average Heat Flux** (kW/cm^2)	20	40.2	532
Pulse Width** (μs)	22	55	22

*The energy radiated to the first wall is defined as the amount of energy radiated for instantaneous values of the heat flux greater than 10% of the maximum.

**The average heat flux is defined as the energy radiated to the first wall divided by the pulse width.

between the initial energy and the energy content of the gas at a temperature of 1 eV. With only 10 MJ initially in the gas, this difference is quite small. For a 30 MJ yield this difference is about 10-20 MJ and for 100 MJ this difference is 80-90 MJ. Hence the average heat flux scales roughly as the difference between the initial fireball energy and 10 MJ rather than just the initial fireball energy.

Such a scaling of the radiant heat flux with fireball energy should also be affected by the cavity radius. For a 6 m cavity radius the gas does not begin radiating to the first wall until the thermal wave reaches it. The results of varying the cavity radius are given in Table 9. These results indicate the fact that once the cavity radius is greater than 6 m the fireball becomes transparent before the thermal wave reaches the wall. This is similar to the results at high gas pressure. This effect is clearly demonstrated in Fig. 12 and Fig. 13. These are snapshot plots of the plasma and the radiation temperatures at different times. Note that at 12.8 μs and 406 μs the radiation temperature is uniform throughout the cavity, indicating that the transparency limit has been reached. This occurs at very nearly the same time that the thermal wave reaches 6 m in radius. Surprisingly, the 8 m and 12 m cavity heat flux results do not scale as R^{-2}. Even though the fireball becomes transparent before reaching the wall in each case, there is a difference in the rate of radiation to the wall. This is almost a factor of two faster in the 12 m cavity. Hence the heat flux on the 12 m cavity wall is not $(8/12)^2$ times less than in the 8 m cavity, but is only about 20% less.

In Table 10, we compare the response of 0.25 torr of Xe to Ar for a 30 MJ fireball. The overpressures in each case are negligible. The fundamental

Table 9

Comparison of Different Cavity Radii for a 30 MJ Fireball in 1/4 Torr of Xenon

	Cavity Radius		
	6 m	8 m	12 m
Gas Type	Xe	Xe	Xe
Gas Pressure (0°C) (torr)	0.25	0.25	0.25
Energy Deposited (MJ)	30	30	30
Initial Fireball Radius (m)	1	1	1
Initial Fireball Temperature (eV)	23.5	23.5	23.5
Initial Gas Temperature (eV)	0.1	0.1	0.1
Maximum Overpressure (torr)	13.7	4.2	1.4
Time of Maximum Overpressure (μs)	23	1000	1000
Energy Radiated to the First Wall*(MJ)	10	11.1	12.4
Average Heat Flux**(kW/cm^2)	40.2	13.8	11.4
Pulse Width** (μs)	55	100	60

*The energy radiated to the wall is defined as the amount of energy radiated for instantaneous values of the heat flux greater than 10% of the maximum.

**The average heat flux is defined as the energy radiated to the first wall divided by the pulse width.

Table 10

Comparison of the Response of Xenon and Argon to a 30 MJ Fireball

	Xe	Ar
Cavity Radius (m)	6	6
Gas Pressure (0°C) (torr)	0.25	0.25
Energy Deposited (MJ)	30	30
Initial Fireball Radius (m)	1	1
Initial Fireball Temperature (eV)	23.5	26
Initial Gas Temperature (eV)	0.1	0.1
Maximum Overpressure (torr)	13.7	16.0
Time of Maximum Overpressure (μs)	23	9.5
Energy Radiated to First Wall* (MJ)	10	11.9
Average Heat Flux**	40.2	105
Pulse Width**	55	25

* The energy radiated to the wall is defined as the amount of energy radiated for instantaneous values of the heat flux greater than 10% of the maximum.

** The average heat flux is defined as the energy radiated to the first wall divided by the pulse width.

dynamics of the fireball is the same for each gas, but the higher heat capacity of xenon allows it to hold the radiant energy better than argon. The average heat flux for argon, once the thermal wave reaches the wall, is about 2.5 times as large as for xenon. However, this makes little difference in the thermal response of the wall because the width of the heat pulse in both cases is quite small compared to the thermal time constant of most wall materials.

Finally, Table 11 is a comparison of the response of 0.25 torr of argon and 50 torr of argon in a 4 meter cavity for a 30 MJ fireball. As noted many times before, the fireball behavior is very different for these two gas pressures and this cavity radius. In the high pressure case, the overpressure at the wall is substantial and the heat flux is lower. In the low pressure case, the overpressure is negligible and the heat flux is very large. Solid first walls can be designed to handle the high overpressure/low heat flux conditions but the low overpressure/high heat flux conditions must be accommodated by increasing the cavity radius or placing a sacrificial material in front of the structural wall.

Table 11

Comparison of the Response of 0.25 torr Argon and 50 torr Argon to a 30 MJ Fireball in a 4 Meter Cavity

	1/4 torr	50 torr
Cavity Radius (m)	4	4
Gas Type	Ar	Ar
Energy Deposited (MJ)	30	30
Initial Fireball Radius (m)	1	0.10
Initial Fireball Temperature (eV)	26	64
Initial Gas Temperature (eV)	0.1	0.1
Maximum Overpressure (torr)	13.7	1140
Time of maximum overpressure (μs)	23	2000
Energy radiated to first wall* (MJ)	10	7.5
Average Heat Flux** (kW/cm^2)	40.2	15
Pulse Width** (μs)	55	248

*The energy radiated to the first wall is defined as the amount of energy radiated for instantaneous values of the heat flux greater than 10% of the maximum.

**The average heat flux is defined as the energy radiated to the wall divided by the pulse width.

Conclusions of Low Pressure Results

(1) For target yields of 100-1000 MJ, cavity radii of 6-12 m, initial fireball radii of 1-5 m and a gas pressure of 0.25 torr when measured at 0°C, inert cavity gases do not act as a thermal capacitor to hold up the energy of the microexplosion. Large instantaneous heat fluxes on the first wall lead to unacceptable temperature transients and thermal stress levels.

(2) The behavior of the fireball in the low pressure cavity is different from the high pressure case. The radiation mean free paths in the fireball and outside the fireball are long. The mean free paths in the temperature gradient between hot and cold regions are short. Consequently, the fireball does not drive a shock wave to the first wall, but instead a supersonic thermal wave propagates through a motionless gas. Once this opaque region of plasma in the temperature gradient reaches its transparency temperature, the fireball volumetrically radiates to the first wall. This combination of effects results in very high instantaneous heat fluxes but very low overpressures at the first wall.

(3) Xenon produces a first wall heat flux about 2.5 times less than argon under similar conditions.

(4) The heat flux at the first wall increases dramatically when the fireball energy is increased from 30 MJ to 100 MJ. This is because the heat flux is proportional to the difference between the fireball initial energy and about 10 MJ rather than just the absolute magnitude of the fireball energy.

(5) Increasing the radius of the initial fireball, determined by the pellet output spectra, reduces the heat flux on the first wall by increasing

the width of the radiation pulse. However, only a factor of three reduction is achieved between fireball radii of 1 and 3 meters.

(6) The heat flux incident on the first wall does not decrease as R^{-2} as the cavity radius increases. It decreases at a substantially slower rate because there is a thermal interaction between the gas near the first wall and the transparent radiating fireball. More energy is radiated from the fireball in the short X-ray burst when the wall is further from the fireball.

(7) In general, these results indicate that noble gases will not protect the first wall in laser fusion reactors from excessively large surface heat loads and the subsequently large thermal stresses or evaporation.

Implications of Results

The results presented in this paper indicate that noble gases, such as argon and xenon, may not be suitable for first wall protection in either light ion beam reactors or laser fusion reactors. In the case of light ion beams, calculations also indicate that non-noble gases, polyatomic gases, perform well in protecting the first wall. Hence, our general conclusion is that gas protection looks very attractive for light ion beam fusion since there is no restriction on the gas type and conventional first wall design appears to be acceptable.

However, for laser fusion applications it is thought that noble gases are particularly important because they have a higher resistance to laser induced gas breakdown than polyatomic gases. If noble gases are indeed required for laser fusion cavities, then first wall designs that can accommodate the high heat flux must be used. These will likely consist of a sacrificial

shield, or liner, in front of the structural first wall.[30] This concept has been studied previously for systems with no protection mechanism or only a partial protection such as magnetic fields which do not affect the pellet X-rays. Further analysis of the walls in gas protected laser fusion cavities should not rely upon the "thermal capacitor" effect of the gas which was incorrectly postulated.

Acknowledgement

This work was supported by Sandia Laboratory under Contract #DSG/06-9329.

References

1. J. Nuckolls, et al., "Laser Compression of Matter to Super High Densities: Thermonuclear (CTR) Applications", Nature 29, 139 (1972).

2. K. Brueckner and S. Jorna, "Laser-Driven Fusion", Rev. Mod. Phys. 46, 325 (1974).

3. G. R. Magelssen and G. A. Moses, "Pellet X-Ray Spectra for Laser Fusion Reactor Designs", Nucl. Fus. 19, 301 (1979).

4. R. W. Conn, "First Wall and Divertor Plate Material Selection in Fusion Reactors", J. Nucl. Mat. 76&77, 103 (1978).

5. G. Kulcinski, "First Wall Protection Schemes for ICF Reactors", J. Nucl. Mat. 85&86, 87 (1979).

6. L. A. Booth, "Central Station Power Generation by Laser Driven Fusion", LA-4858-MS, Los Alamos Scientific Laboratory (1972).

7. D. A. Freiwald, et al., "Laser Fusion Generating Stations Based on the Magnetic Protected Reactor Cavity", LA-UR-75-2035, Los Alamos Scientific Laboratory; also Trans. ANS 22, 68 (1975).

8. J. A. Maniscalco and W. R. Meier, "Liquid-Lithium Waterfall Inertial Confinement Fusion Reactor Concept,"Trans. ANS 26, 62 (1977).

9. M. Monsler, et al., "Electric Power from Laser Fusion: The HYLIFE Concept", Trans. ANS 30, 21 (1978).

10. R. W. Conn, et al., "SOLASE, A Laser Fusion Reactor Study", University of Wisconsin Fusion Engineering Program Report UWFDM-220, 1978.

11. G. A. Moses, et al., "The SOLASE Conceptual Laser Fusion Reactor Study", Proc. 3rd ANS Top. Meeting on Fusion Tech., p. 448.

12. S. I. Abdel-Khalik, "Engineering Problems of Laser Driven Fusion Reactors", Nucl. Tech. 43, 5 (1979).

13. D. L. Cook and M. A. Sweeney, "Design of Compact Particle Beam Driven Inertial Confinement Fusion Reactors", Proc. 3rd ANS Top. Meeting on Fusion Tech., p. 1178.

14. G. Yonas, "Fusion Power with Particle Beams", Sci. Am. 239, 50 (Nov. 1978).

15. G. Taylor, Proc. R. Soc. A201, 159 (1950).

16. V. Zeldovich and Y. Raizer, Physics of Shock Waves and High Temperature Hydrodynamic Phenomena, Academic Press (New York, 1966), Vol. I and II.

17. J. Von Neumann and R. Richtmyer, "A Method for the Numerical Calculation of Hydrodynamic Shocks", J. Appl. Phys. 21, 232 (1950).

References (cont.)

18. R. Richtmyer and K. Morton, Difference Methods for Initial Value Problems, Wiley (New York, 1967, 3nd Ed.), p. 323.

19. G. Fraley, et al., "Thermonuclear Burn Characteristics of Compressed Deuterium-Tritium Microspheres", Phys. Fld. 17, 474 (1974). (Appendix B).

20. L. Spitzer, "The Physics of Fully Ionized Gases", Interscience Publishers, (New York, 1962).

21. G. A. Moses, "PHD-I, A Plasma Hydrodynamics Computer Code", University of Wisconsin Fusion Engineering Program Report UWFDM-160, 1976.

22. R. Kidder and W. Barnes, "WAZER - A One-Dimensional, Two Temperature Hydrodynamic Code", Lawrence Livermore Laboratory Report UCRL-50583.

23. S. L. Thompson, "Improvements in the CHART-D Energy Flow Hydrodynamic Code V: 1972/73 Modifications", SLA-73-0477, Sandia Laboratories (1973).

24. Ref. 16, Chapter V.

25. R. R. Peterson and G. A. Moses, "MFP-A Calculation of Radiation Mean Free Paths, Ionization and Internal Energies in Noble Gases", University of Wisconsin Fusion Engineering Program Report UWFDM-307 (1979). (Submitted for publication to Computer Physics Communications.)

26. D. L. Cook, private communication.

27. R. Bangerter and D. Meeker, "Ion Beam Inertial Fusion Target Designs", Presented at Faculty Workshop on ICF Fusion, Argonne National Laboratory, June 5-9, 1978.

28. E. Lovell and R. Engelstad, "First Wall Mechanical Design for Light Ion Beam Fusion Reactors", University of Wisconsin Fusion Engineering Program Report UWFDM-322, Nov. 1979. (Submitted for publication to Nuclear Technology.)

29. T. O. Hunter and G. L. Kulcinski, "Description of the Reponse of Material to Pulsed Thermonuclear Radiation - Effect of Gases on Modification of Pellet Debris Spectra and First Wall Response", University of Wisconsin Fusion Engineering Report UWFDM-232, April 1978.

30. R. W. Conn, et al., "Studies of the Technological Problems of Laser Driven Fusion Reactors, The Pre-SOLASE Design", University of Wisconsin Fusion Engineering Program Report UWFDM-190, December 1976.

Figure Captions

Fig. 1 - Schematic history of blast wave. (a) Initially, radiation mean free paths ℓ are short at the shock front; fireball remains trapped behind the shock. (b) Fireball expands; temperature drops below $T_{transparent}$; ℓ becomes long at the shock front; radiation leaks to the first wall. (c) Temperature, lowered because of radiant heat loss, is so low that radiant heat transfer ceases and the fireball remains fixed in the gas while the shock hits the first wall.

Fig. 2 - Equilibrium gas and radiation specific energies for argon at $N = 1.67 \times 10^{18} cm^{-3}$ and $6.0 \times 10^{17} cm^{-3}$.

Fig. 3 - Planck mean free path in argon at $N = 2.7 \times 10^{19} cm^{-3}$.

Fig. 4 - Gas temperature profiles at various times for a 30 MJ explosion in $1.67 \times 10^{18} cm^{-3}$, 0.1 eV argon gas.

Fig. 5 - Gas pressure profiles at various times for a 30 MJ explosion in $1.67 \times 10^{18} cm^{-3}$, 0.1 eV argon gas.

Fig. 6 - Pressure and heat flux at a 4 meter radius first wall. A 30 MJ explosion sends a blast wave through $1.67 \times 10^{18} cm^{-3}$, 0.1 eV argon gas.

Fig. 7 - Rosseland and Planck mean free paths for radiation in $1.67 \times 10^{18} cm^{-3}$ argon. The radiation is assumed to be in equilibrium with the gas so that $T_r = T_p = T$.

Fig. 8 - Propagation of 30 MJ of energy through a $1.67 \times 10^{18} cm^{-3}$, 0.1 eV argon gas. The positions of the boundaries of 50 Lagrangian zones are plotted against time as is the position of a shock front predicted by strong shock theory.

Fig. 9 - Pressure and heat flux at a 4 meter radius first wall. A 30 MJ blast wave propagates through 1.67×10^{-18}, 0.1 eV "diatomic argon" gas. The radiation mean free paths are those of argon except when $T_r < 1.5$ eV, where they are limited to 50 cm.

Fig. 10 - Pressure and heat flux at a 6 meter first wall. A 30 MJ blast wave propagates through $8.88 \times 10^{15} cm^{-3}$, 0.1 eV xenon gas.

Fig. 11 - Gas temperature (solid line), radiation temperature (- -) and Planck mean free path (- . -) profiles at t = 0.65 μsec for a 30 MJ blast wave propagating through $8.88 \times 10^{15} cm^{-3}$, 0.1 eV xenon gas.

Fig. 12 - Gas temperature profiles at t = 12.8 μsec at t = 406 μsec for a 30 MJ explosion in $8.88 \times 10^{15} cm^{-3}$, 0.1 eV xenon gas.

Fig. 13 - Radiation temperature profiles at t = 12.8 μsec and t = 406 μsec for a 30 MJ explosion in $8.88 \times 10^{15} cm^{-3}$, 0.1 eV xenon gas.

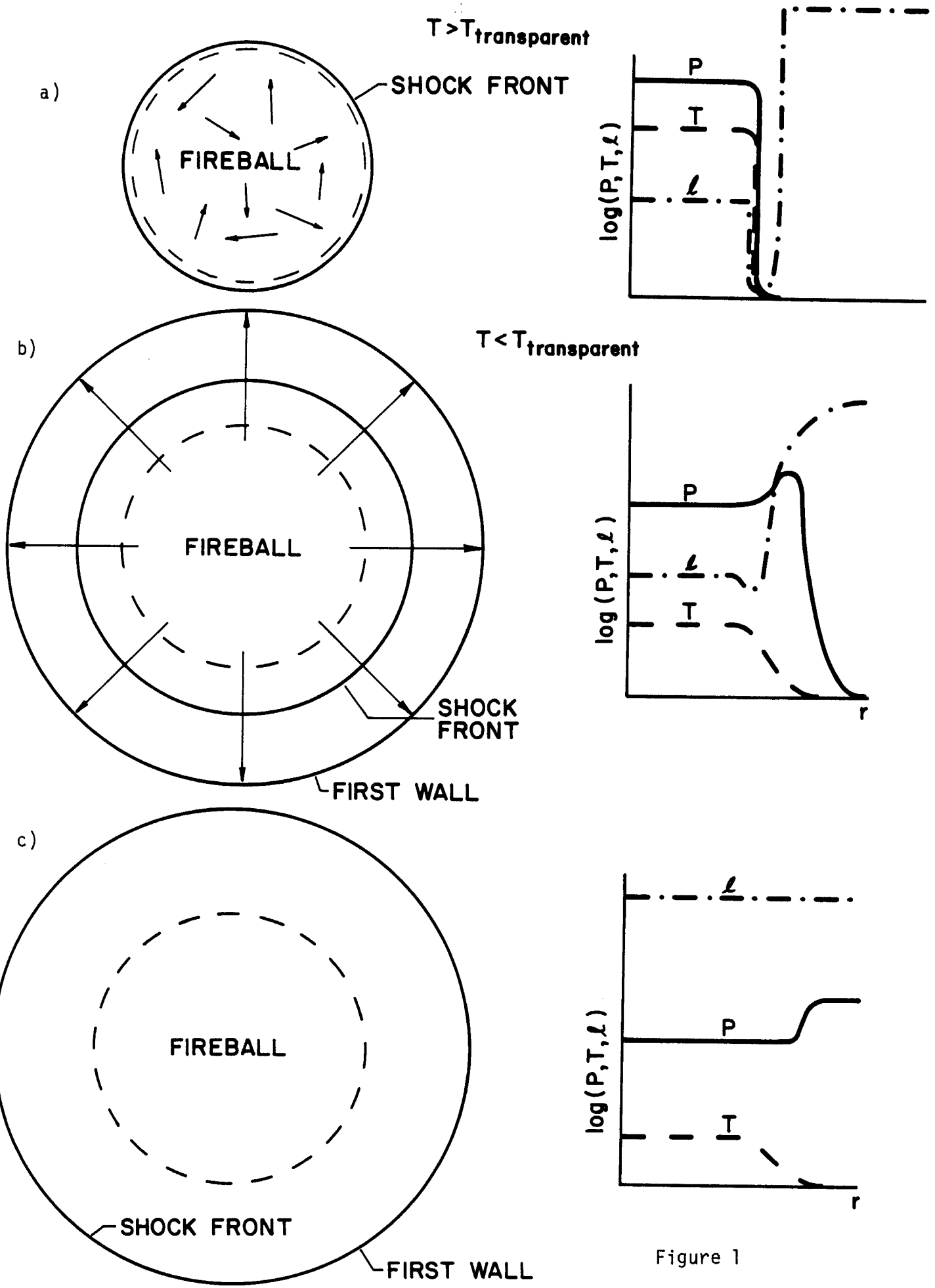
a)
FIREBALL
SHOCK FRONT
T>T transparent
P
T
ℓ
log(P,T,ℓ)
b)
FIREBALL
SHOCK FRONT
FIRST WALL
T<T transparent
P
ℓ
T
log (P,T,ℓ)
r
c)
FIREBALL
SHOCK FRONT
FIRST WALL
ℓ
P
T
log(P,T,ℓ)
r

Figure 1

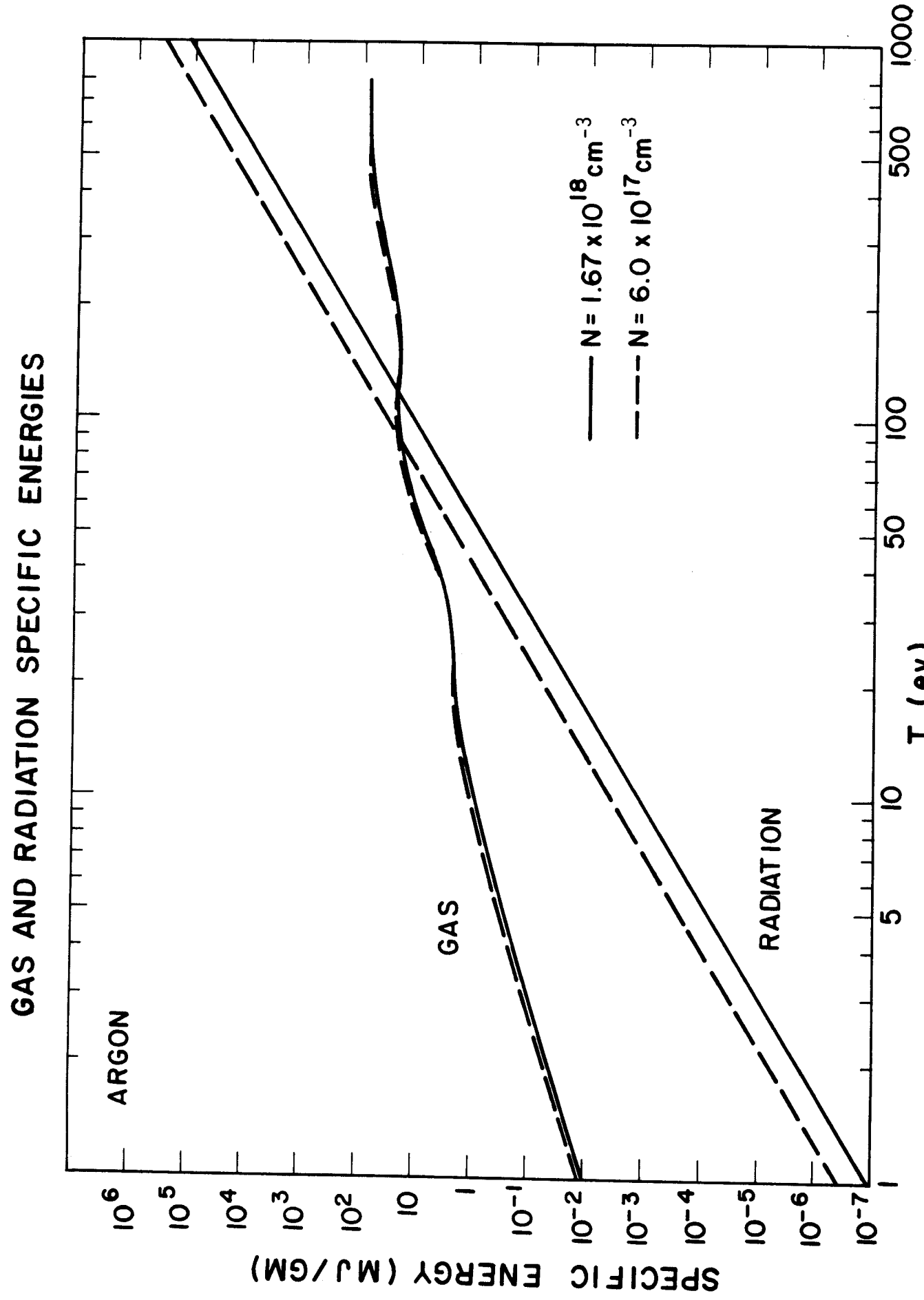
GAS AND RADIATION SPECIFIC ENERGIES
ARGON
GAS
RADIATION
N= 1.67 x 10^18 cm^-3
N= 6.0 x 10^17 cm^-3
SPECIFIC ENERGY (MJ/GM)
T (ev)
10^6
10^5
10^4
10^3
10^2
10
1
10^-1
10^-2
10^-3
10^-4
10^-5
10^-6
10^-7
1
5
10
50
100
500
1000

Figure 2

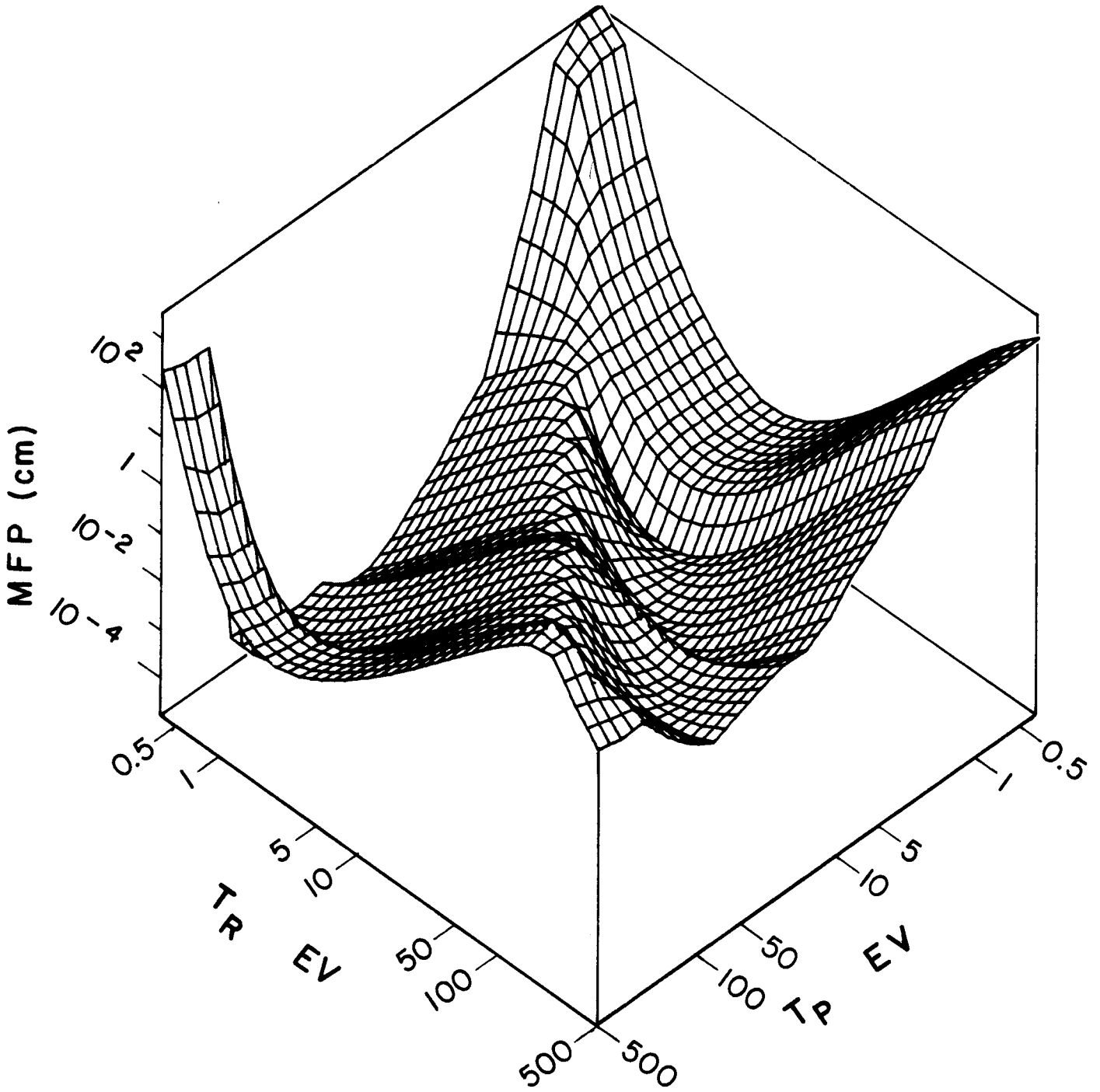

PLANCK MFP
ARGON DENSITY 2.7×10^{19} cm^{-3}

Figure 3

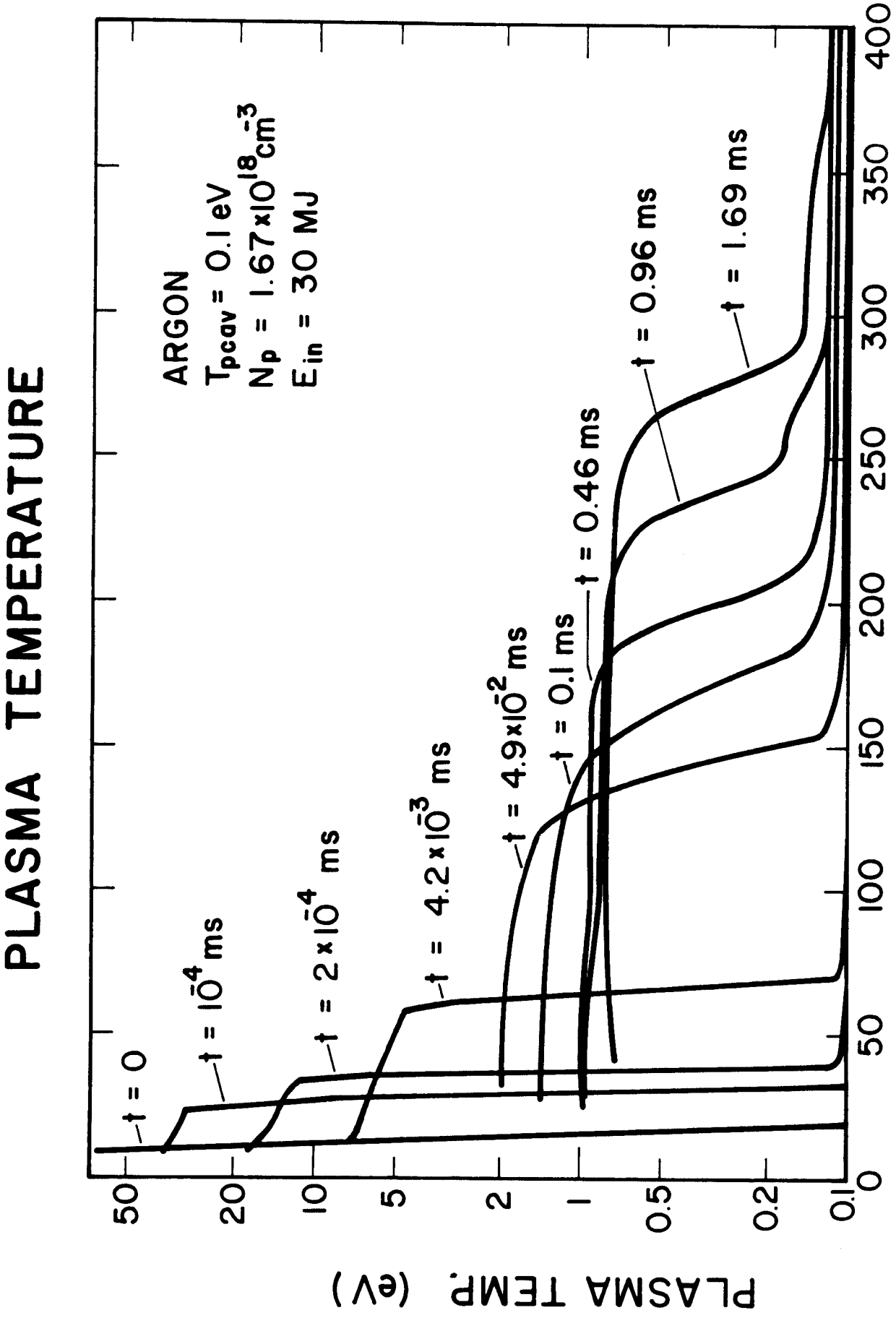
PLASMA TEMPERATURE
ARGON
T_{pcav} = 0.1 eV
N_p = 1.67x10^{18}cm^{-3}
E_{in} = 30 MJ
t = 0
t = 10^{-4} ms
t = 2x10^{-4} ms
t = 4.2x10^{-3} ms
t = 4.9x10^{-2} ms
t = 0.1 ms
t = 0.46 ms
t = 0.96 ms
t = 1.69 ms
PLASMA TEMP. (eV)
50
20
10
5
2
1
0.5
0.2
0.1
0
50
100
150
200
250
300
350
400
RADIUS (cm)

Figure 4

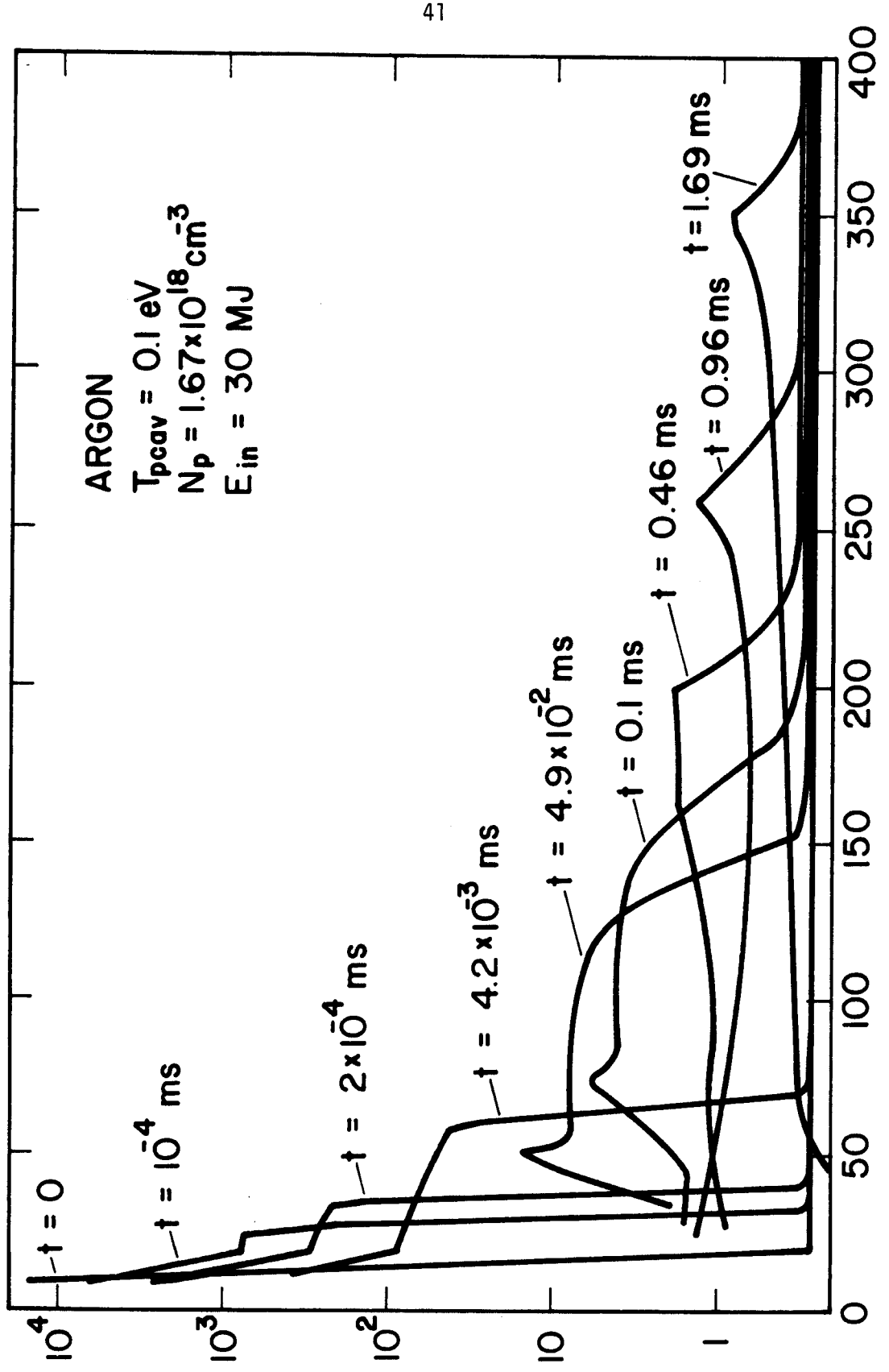
PLASMA PRESSURE
ARGON
T_{pcav} = 0.1 eV
$N_p = 1.67 \times 10^{18} cm^{-3}$
E_{in} = 30 MJ
t = 0
$t = 10^{-4}$ ms
$t = 2 \times 10^{-4}$ ms
$t = 4.2 \times 10^{-3}$ ms
$t = 4.9 \times 10^{-2}$ ms
t = 0.1 ms
t = 0.46 ms
t = 0.96 ms
t = 1.69 ms
PLASMA PRESS. (atm)
10^4
10^3
10^2
10
1
0
50
100
150
200
250
300
350
400
RADIUS (cm)

Figure 5

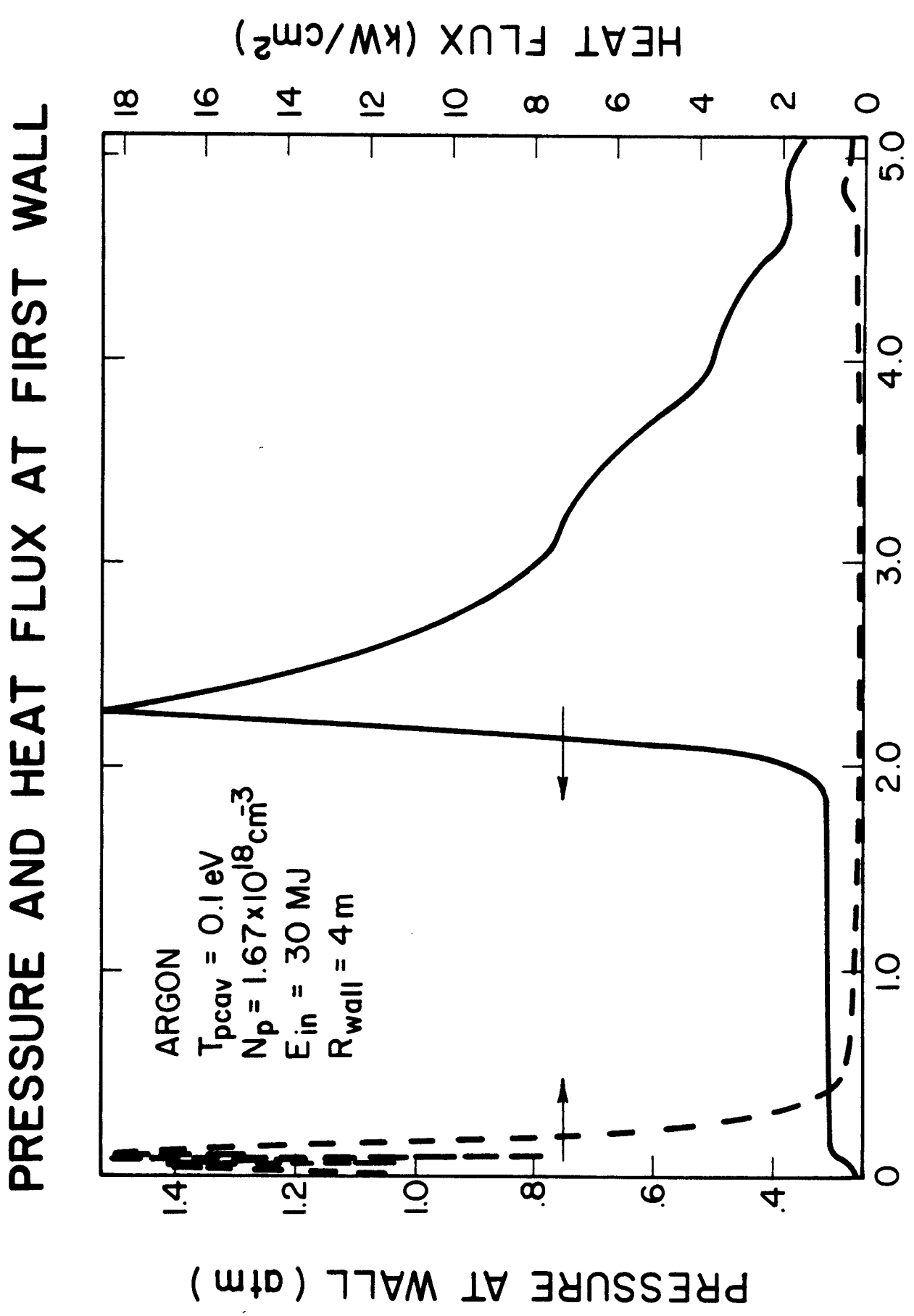
PRESSURE AND HEAT FLUX AT FIRST WALL
ARGON
T_{pcav} = 0.1 eV
N_p = 1.67x10^{18}cm^{-3}
E_{in} = 30 MJ
R_{wall} = 4 m
PRESSURE AT WALL (atm)
HEAT FLUX (kW/cm^2)
TIME (msec)
0
1.0
2.0
3.0
4.0
5.0
.4
.6
.8
1.0
1.2
1.4
0
2
4
6
8
10
12
14
16
18

Figure 6

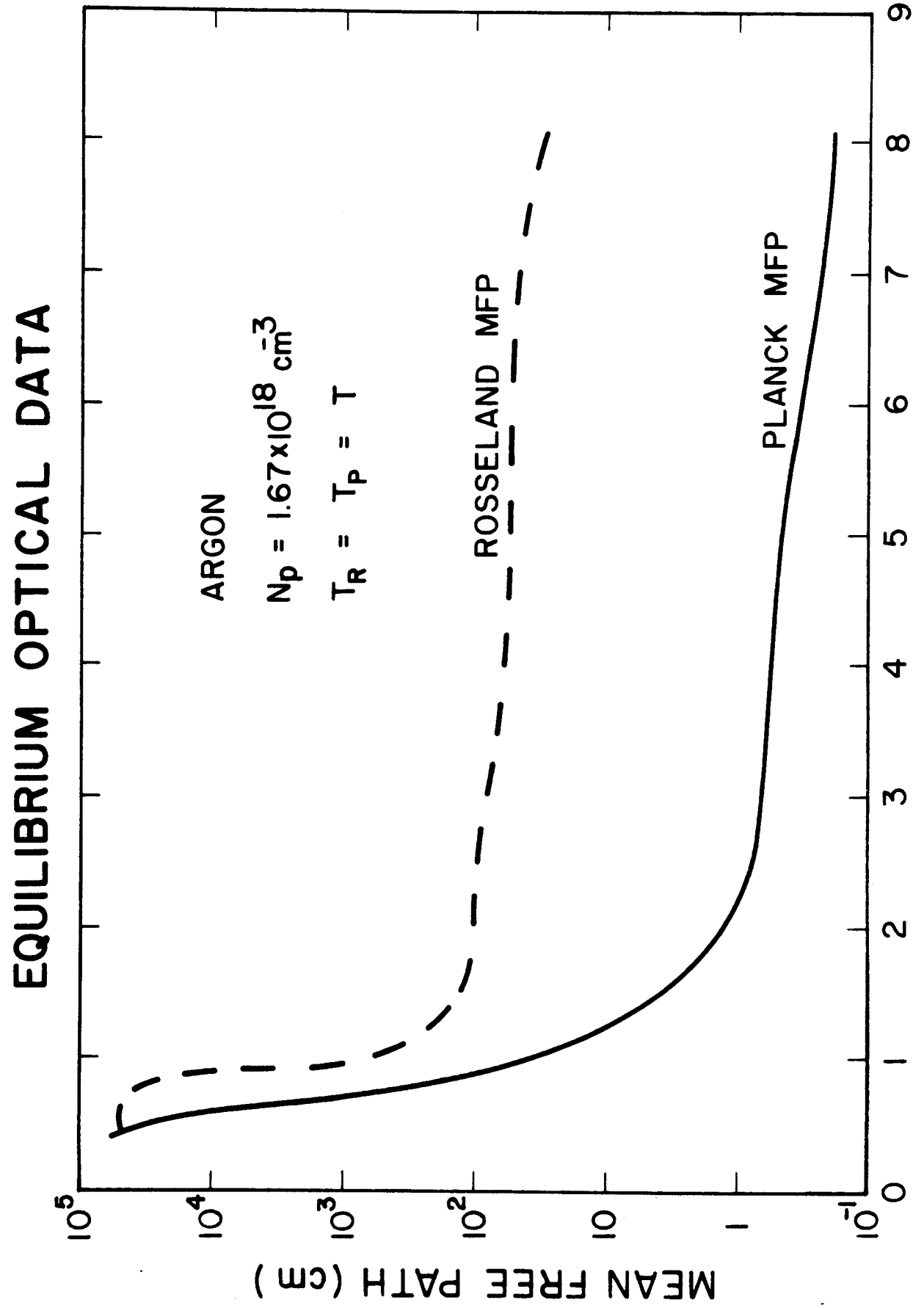
EQUILIBRIUM OPTICAL DATA
ARGON
$N_p = 1.67 \times 10^{18}\ cm^{-3}$
$T_R = T_P = T$
ROSSELAND MFP
PLANCK MFP
MEAN FREE PATH (cm)
10^5
10^4
10^3
10^2
10
1
10^{-1}
0
1
2
3
4
5
6
7
8
9
TEMPERATURE T (eV)

Figure 7

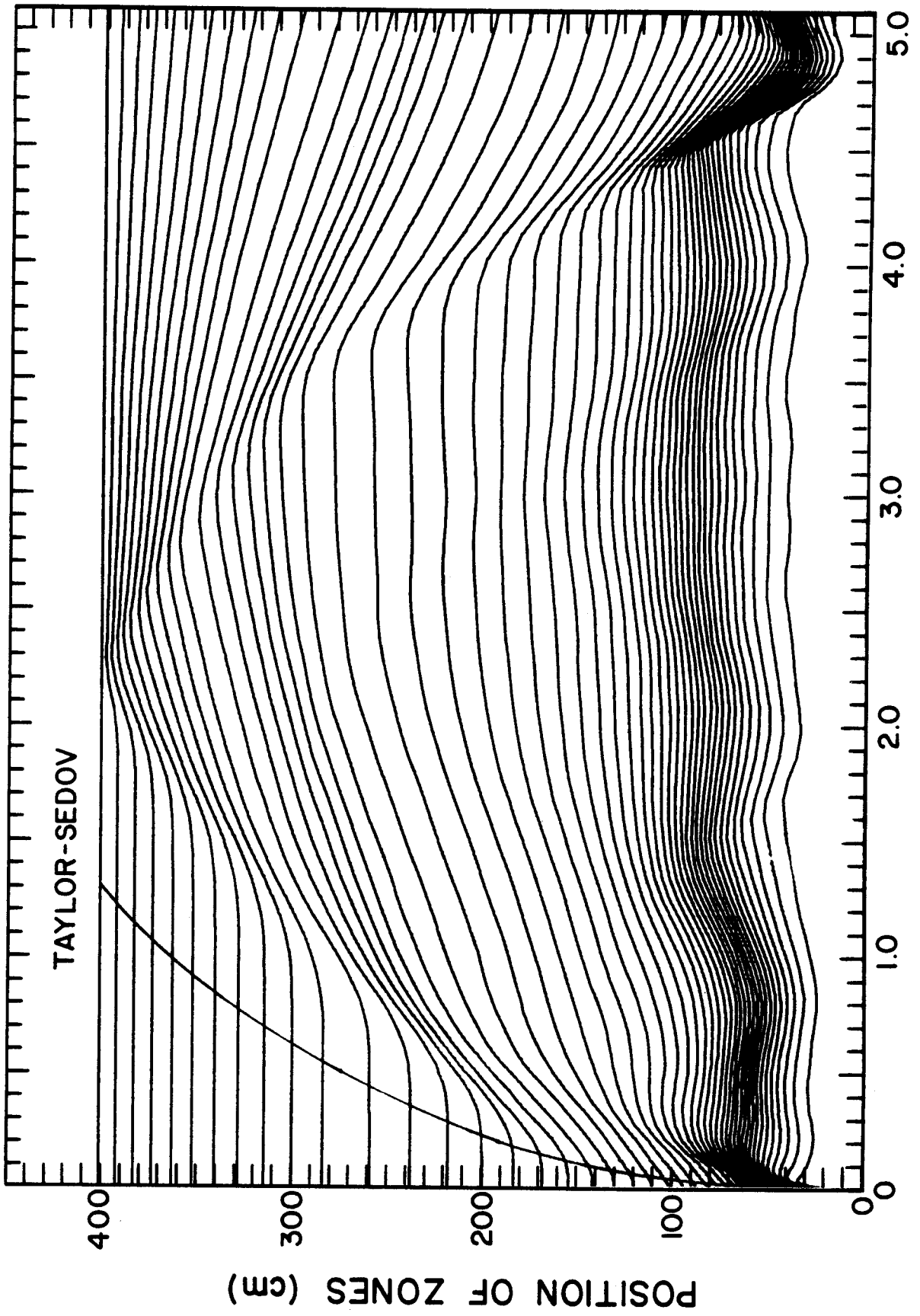
SHOCK PROPAGATION IN ARGON
T_{pcav} = 0.1 eV , N_p = 1.67x10^{18}cm^{-3} , E_{in} = 30 MJ
TAYLOR-SEDOV
POSITION OF ZONES (cm)
400
300
200
100
0
0
1.0
2.0
3.0
4.0
5.0
TIME (msec)

Figure 8

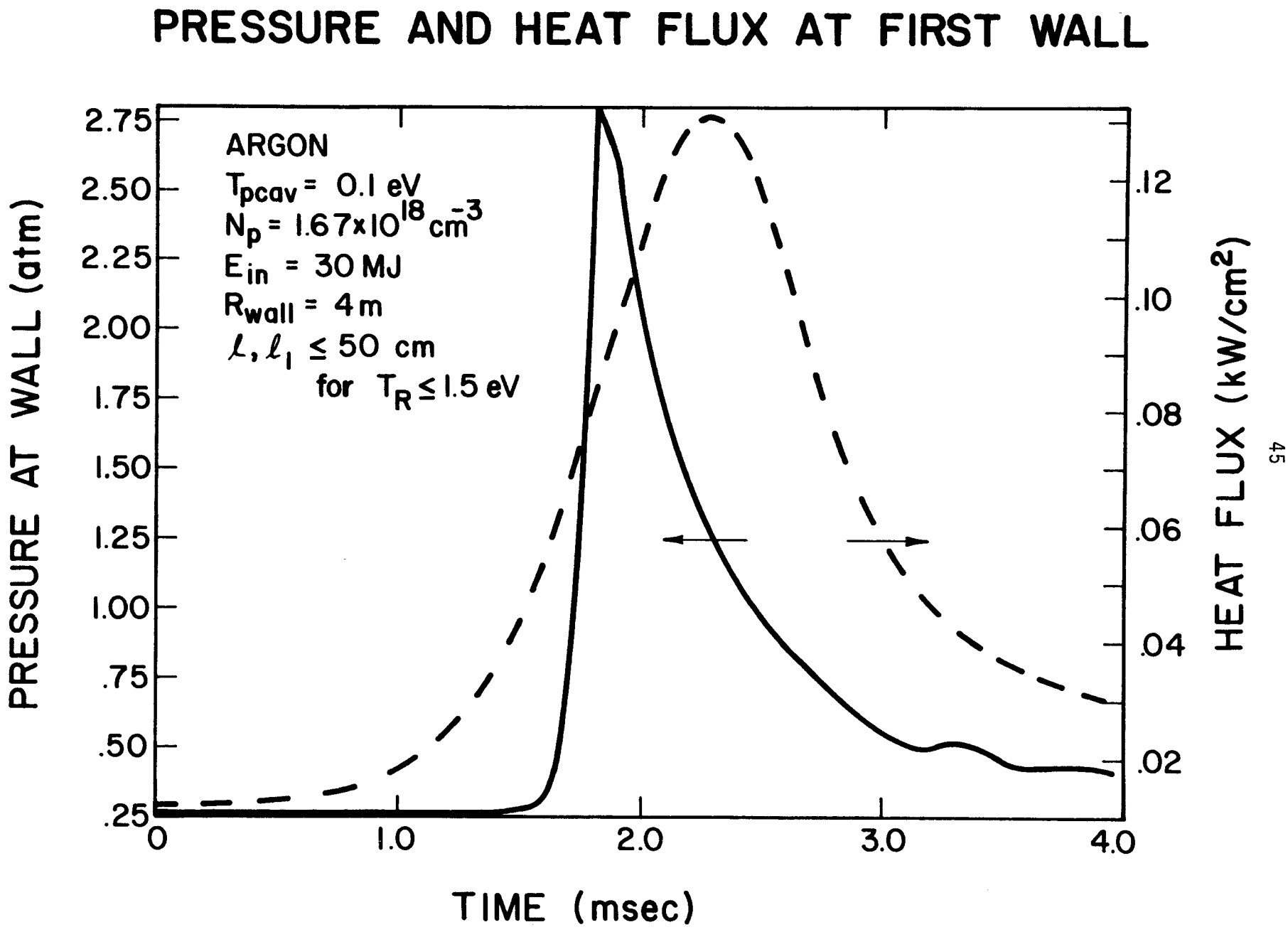
PRESSURE AND HEAT FLUX AT FIRST WALL
ARGON
T_{pcav} = 0.1 eV
$N_p = 1.67 \times 10^{18}$ cm^{-3}
E_{in} = 30 MJ
R_{wall} = 4 m
$\ell, \ell_1 \leq 50$ cm
for $T_R \leq 1.5$ eV
PRESSURE AT WALL (atm)
HEAT FLUX (kW/cm^2)
TIME (msec)
2.75
2.50
2.25
2.00
1.75
1.50
1.25
1.00
.75
.50
.25
.12
.10
.08
.06
.04
.02
0
1.0
2.0
3.0
4.0

Figure 9

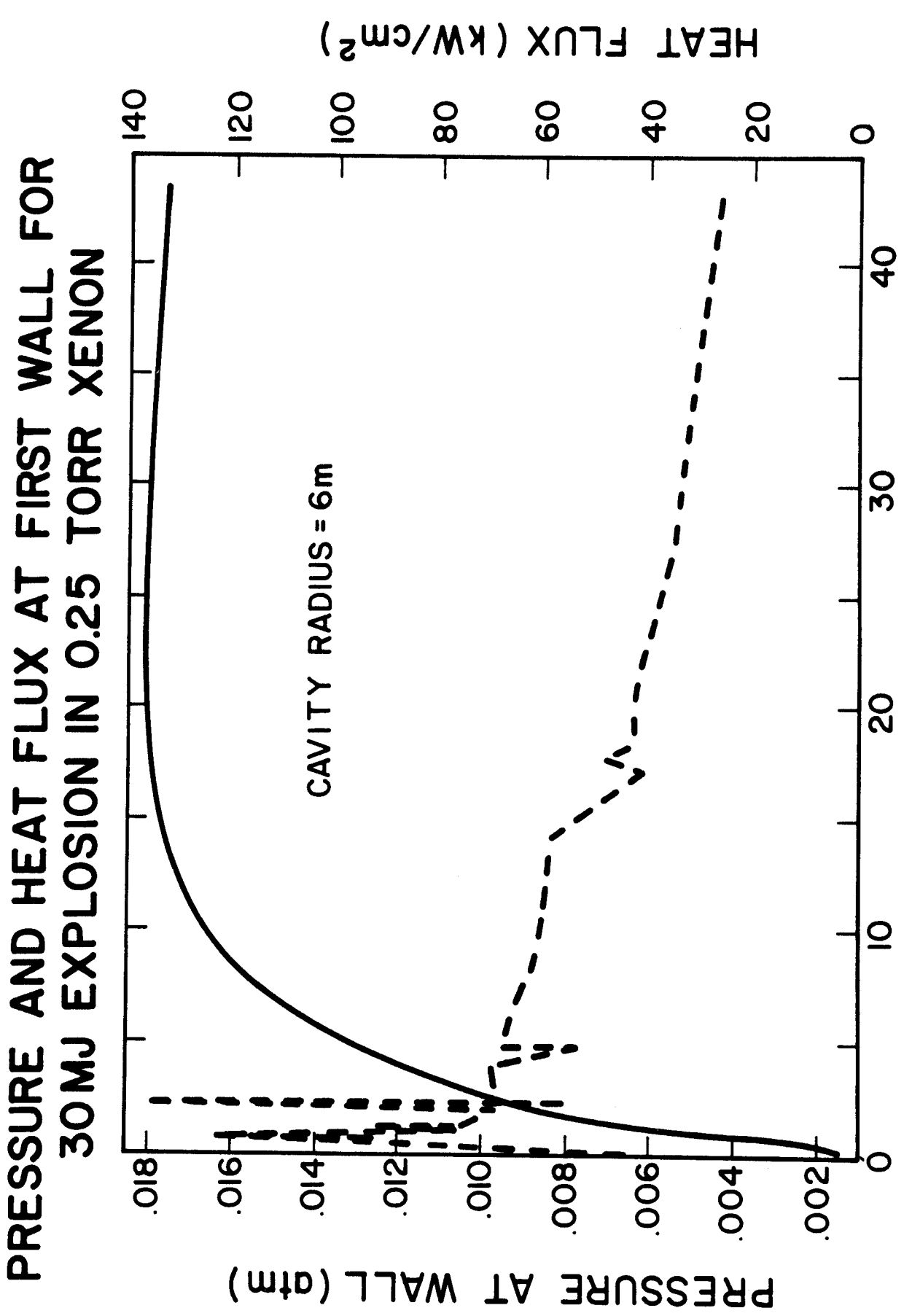
PRESSURE AND HEAT FLUX AT FIRST WALL FOR
30 MJ EXPLOSION IN 0.25 TORR XENON
CAVITY RADIUS = 6m
PRESSURE AT WALL (atm)
HEAT FLUX (kW/cm²)
TIME (μsec)
.018
.016
.014
.012
.010
.008
.006
.004
.002
140
120
100
80
60
40
20
0
0
10
20
30
40

Figure 10

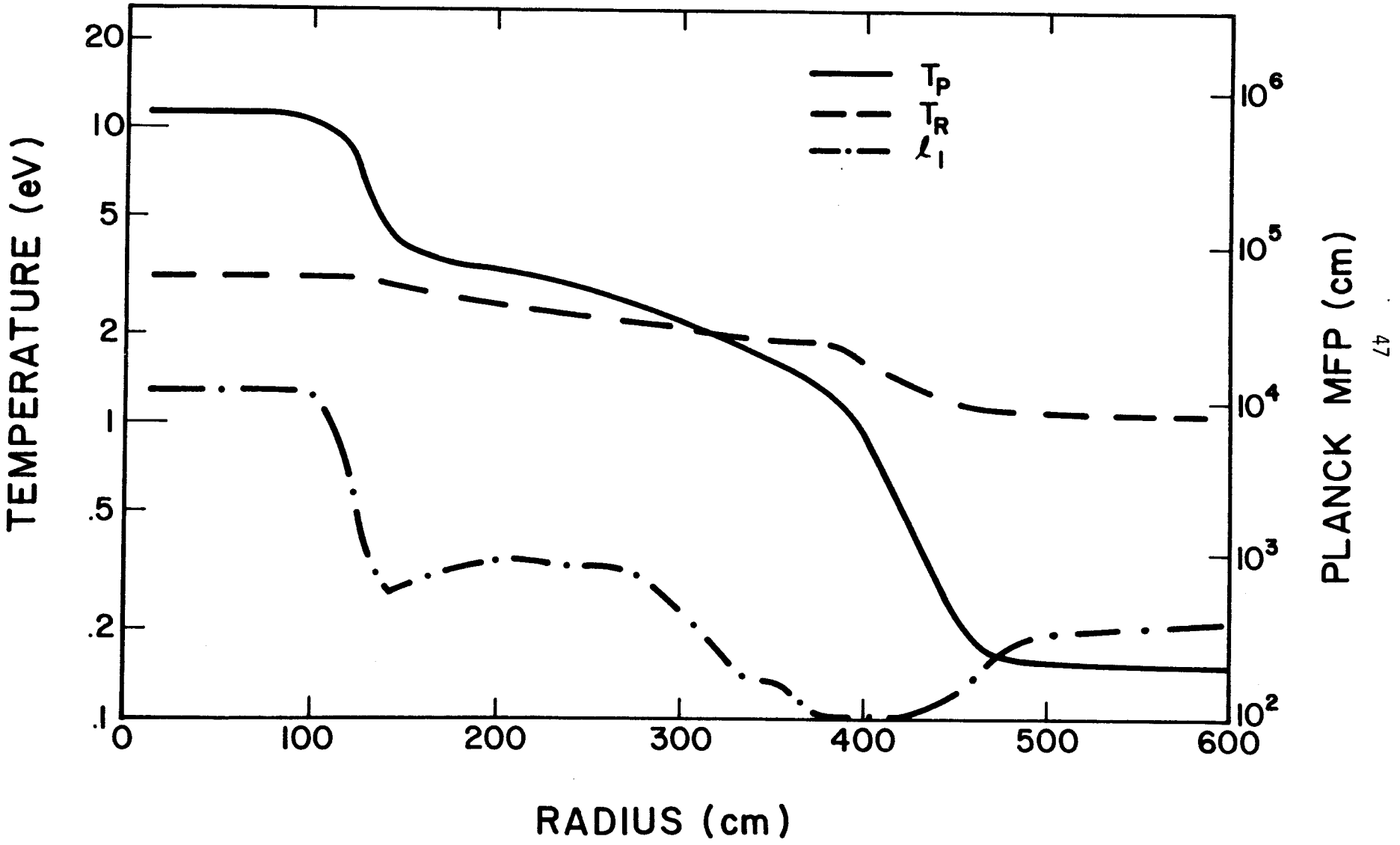
PLASMA TEMPERATURE, RADIATION TEMPERATURE, AND PLANCK MFP AT 0.65 μs FOR 30 MJ EXPLOSION IN 0.25 TORR OF XENON
TEMPERATURE (eV)
20
10
5
2
1
.5
.2
.1
T_P
T_R
ℓ_1
10^6
10^5
10^4
10^3
10^2
PLANCK MFP (cm)
0
100
200
300
400
500
600
RADIUS (cm)

Figure 11

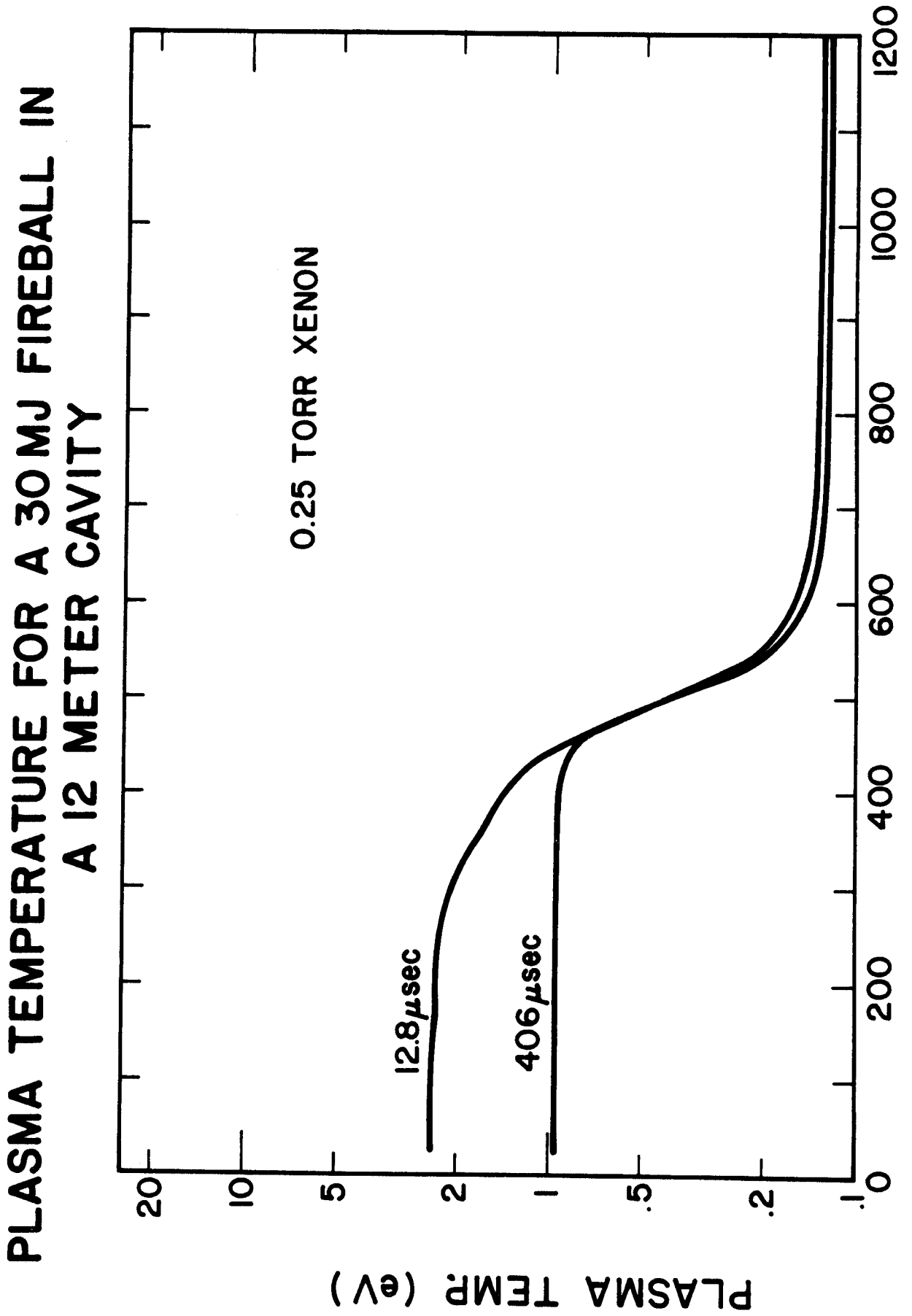
PLASMA TEMPERATURE FOR A 30 MJ FIREBALL IN A 12 METER CAVITY
0.25 TORR XENON
12.8μsec
406μsec
PLASMA TEMP. (eV)
20
10
5
2
1
.5
.2
.1
0
200
400
600
800
1000
1200
RADIUS (cm)

Figure 12

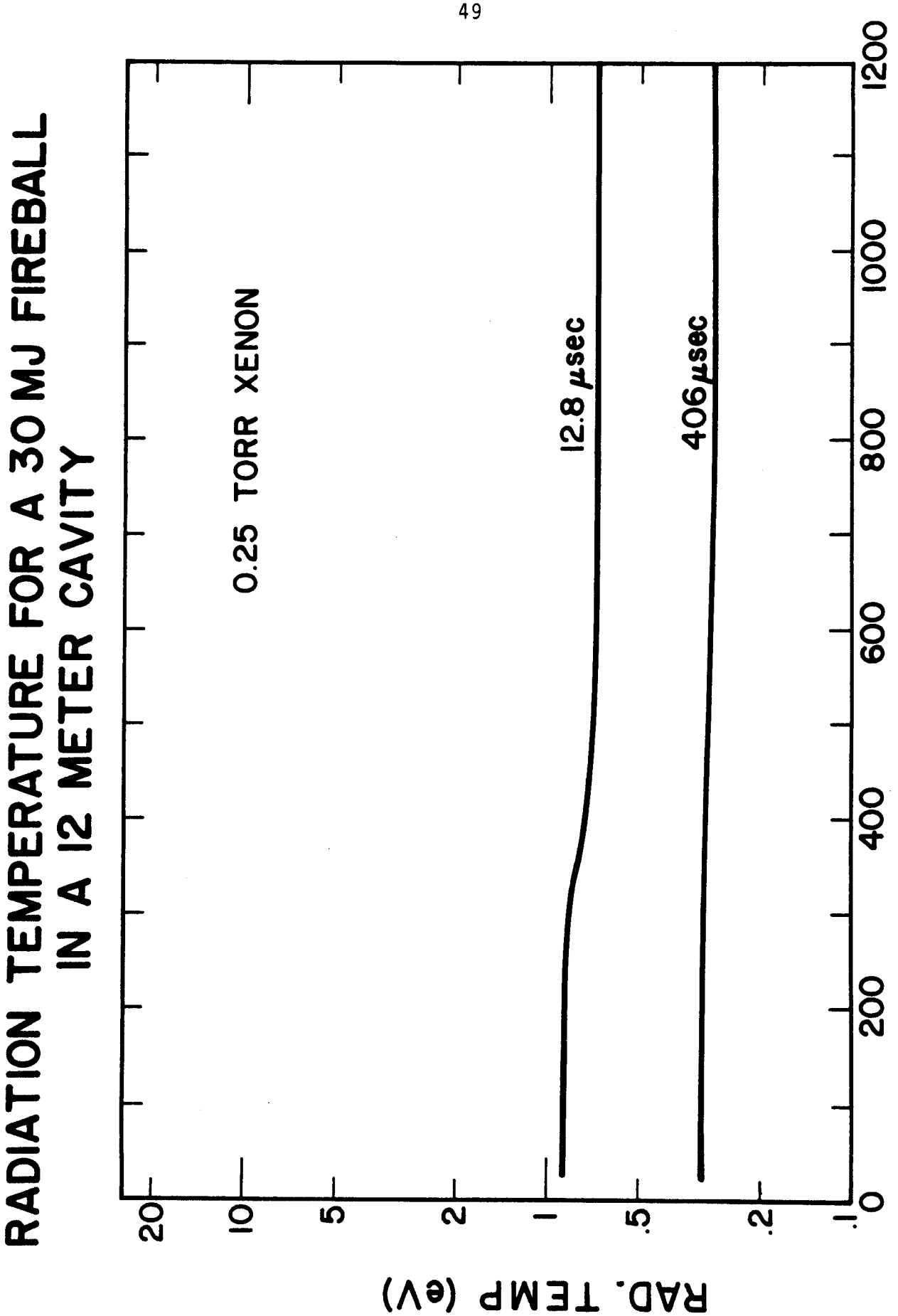
RADIATION TEMPERATURE FOR A 30 MJ FIREBALL
IN A 12 METER CAVITY
0.25 TORR XENON
12.8 μsec
406 μsec
RAD. TEMP (eV)
20
10
5
2
1
.5
.2
.1
0
200
400
600
800
1000
1200
RADIUS (cm)

Figure 13

First Wall Protection in ICF Reactors by Inert Cavity Gases

Gregory A. Moses
Robert R. Peterson

October 1979

UWFDM-323

Fusion Engineering Program
Nuclear Engineering Department
University of Wisconsin
Madison, Wisconsin 53706

This work was supported by Sandia Laboratory under Contract #DSG/06-9329.
Submitted for publication to Nuclear Fusion.

I. Introduction

The inertial confinement approach to controlled thermonuclear fusion involves the compression of the fusion fuel to densities of 1000 times normal liquid density.[1,2] At these high densities, the inertia of the fuel itself and other surrounding tamper material is great enough to hold the fuel together for a time that is longer than the characteristic thermonuclear burn time. If this compression of the fuel is produced in an efficient way, then a net energy gain will result. The compression of the fuel is accomplished by the implosion of spherical fusion pellets by an energy source of high intensity. A variety of different "drivers" have been proposed for the purposes of providing this energy. These include lasers, relativistic electron beams, light ion beams, and heavy ion beams. In each case the beam energy from the driver ablates the outer part of the fusion pellet, creating a force that spherically implodes the inner fuel part of the pellet to thermonuclear ignition conditions. Also, in each case, once the pellet has ignited and burned, it is left in a very explosive condition. About 20%-30% of the fusion energy from the DT reaction is left behind in the pellet. The remainder escapes in the form of 14.1 MeV neutrons. For a pellet energy gain of 100 there is 20-30 times as much internal energy in the pellet following the burn as there was before burning started. Following the thermonuclear burning the pellet violently explodes creating high energy ion debris and X-rays.[3]

These ion debris and X-rays pose serious problems for inertial confinement fusion reactors.[4,5] The ions and X-rays have short mean free paths in solid materials and therefore act as a surface heat source to the reactor first wall.

Furthermore, this heat flux is pulsed and can attain very high instantaneous values. As a result of this problem, the study of inertial confinement fusion (ICF) reactor design has concentrated to a large extent on methods to protect the first wall from this transient surface heat load. In fact the distinguishing feature in each different design is always the first wall protection mechanism. Among the schemes that have been proposed are: the lithium wetted wall[6], the magnetically protected wall[7], the liquid lithium "waterfall" or jets[8,9], and the gas filled cavity[10-13]. In this paper we report an analysis of the gas filled cavity concept for ICF reactor first wall protection. This concept has potential application in at least two forms of ICF, laser fusion and light ion beam fusion.

For laser fusion reactors this concept was proposed in the SOLASE[10-12] design of the University of Wisconsin. In this design a 6 m radius spherical cavity is filled with 0.25-0.5 torr of a noble gas, such as Ne or Xe. The choice of a noble gas is motivated by fears of laser induced gas breakdown as the beams pass through the gas to the target. The first wall in the reactor is graphite. Calculations show that this amount of gas will attenuate the target X-rays and thermalize the ion debris from a representative exploding target before they reach the first wall. It is then postulated that the energy deposited in the gas will be re-radiated to the first wall in a pulse of greater than a millisecond in duration. Such a long pulse can be thermally accommodated by the graphite wall. This behavior is crucial to the feasibility of gas protection in laser fusion reactors as conceived in the SOLASE concept. The gas must act as a "thermal capacitor" to transform heat pulses of nanosecond duration into heat pulses of millisecond duration.

Gas protection of the first wall in a light ion beam fusion reactor[13] comes as a natural consequence of the means to propagate the ion beams from their diodes to the target. In this fusion concept it is proposed to break down ionized channels in a background gas to serve as "renewable electrical connections" between the individual diodes and the target.[14] To meet this need it is estimated that 10-100 torr of gas is required. This is a considerably higher pressure than in the laser fusion case. Therefore, in a light ion beam (LIB) fusion reactor the first wall will be automatically protected from the exploding target. In this high pressure cavity and the low pressure cavity of laser fusion it is essential to understand the behavior of this gas, once the pellet debris has been deposited into it. It must be verified that the gas will actually serve as a thermal capacitor, and if it does, then the detailed dynamics of the gas must be known to design the first wall.

In this paper we report the development of a new computer code to model the response of the cavity gases to the sudden introduction of energy by the exploding pellet. This code is utilized to predict the response of both high pressure (LIB reactors) and low pressure (laser reactors) cavity gases. Particular attention is paid to the behavior of noble gases, but non-noble gas behavior is also included for comparison purposes. Numerous calculations are presented for varying combinations of important parameters so that a catalog of results as a function of these parameters can be assembled. In addition, a detailed look at the basic phenomena that control the gas response in the high and low pressure cases is given. This is necessary because several heretofore unpredicted or unrecognized phenomena are shown to be very important to the gas dynamics. Part II of this paper is a discussion of the high pressure gas filled cavity with applications to LIB fusion and Part III is a similar discussion of the low pressure gas that

is associated with laser fusion. Because the results of each of these cases are quite different, the conclusions and implications of the results are discussed at the end of each part rather than in combination at the end of the paper.

II. High Pressure Cavity Gas - Light Ion Beam Applications

Phenomenology

The cavity gas pressure for light ion beam reactors is estimated to be from 10-100 torr when measured at 0°C. The actual property of importance is the gas number density and this is 3.5×10^{17} to $3.5 \times 10^{18} cm^{-3}$ at this pressure and temperature. The cavity gas temperature will certainly not be 0°C and thus the pressure will be higher than 10-100 torr. However, a convention in this field has been established that the gas density is given in terms of its pressure at 0°C. This convention will be used in all of the following discussions except where specifically noted. This gas density is required to provide a sufficient electron density in the ionized channel that is established between the diode and the target. This is related to the return current that is necessary for current neutralization as the light ion beam propagates down the channel. A detailed discussion of this problem is not important to the considerations in this paper. The major point to be made here is that this gas density will very effectively attenuate the X-ray energy and thermalize the ions that result from the target explosion. For light ion beam targets the X-ray spectrum will have an effective temperature less than 1 keV. Such a blackbody spectrum will be absorbed within 10 cm of the target. Likewise, the ion debris spectra will be soft due to the high Z material in the pellet. It is therefore postulated that the pellet explosion will almost instantaneously put the cavity gas in an initial state characterized by a hot ball of plasma with a radius of ~10 cm at the center of the cavity, surrounded by cold gas out to the first wall. This is the model that is used for all of the high pressure gas calculations.

This model is certainly an idealization of the actual dynamics of the pellet exploding into the gas immediately surrounding it. However, since we expect that the propagation of the pellet energy obeys something resembling strong shock theory[15], the only important initial parameters should be the energy and the mass density. Work is currently underway to study this problem in more detail, but for our analysis the effect of this idealization will only be tested parametrically.

The hot ball of plasma created by the pellet explosion is called a fireball. Fireballs have been studied extensively as part of the nuclear weapons atmospheric testing program[16]. The behavior of fireballs can be described using Fig. 1. The two major ingredients of a fireball are plasma and the radiation field associated with this plasma. Figure 2 shows the energy density of argon plasma at densities of $1.67 \times 10^{18} cm^{-3}$ and $6.0 \times 10^{17} cm^{-3}$ as a function of temperature. Included on this same graph is a plot of the equilibrium radiation energy density that is associated with these plasmas. Both densities are considered because for a gas initially at $1.67 \times 10^{18} cm^{-3}$, the density inside the fireball quickly drops to $6 \times 10^{17} cm^{-3}$. Note that above a temperature of 80 eV the majority of the total energy in the fireball is in the form of radiation. Since radiative energy is more easily transported, it is therefore not surprising that the behavior of this radiation plays a very important role in the fireball dynamics. Figure 1 shows the state of the fireball at three important times in its evolution. Initially the fireball is a hot plasma with its radiation in equilibrium at a temperature T, greater than the transparency temperature

of the plasma. Hence the radiation mean free path is short and all of the fireball energy is "trapped" behind a spherical front that is being pushed outward by the difference in pressure ahead and behind it. This phenomenon is often described by strong shock theory,[15] which predicts that the shock velocity is given by the expression

$$\dot{R}(t) = \frac{2}{3}\,\xi_o\left(\frac{E_{in}}{\rho_o}\right)^{1/5} t^{-3/5} \quad ,$$

where E_{in} is the initial fireball energy, ρ_o is the initial gas density, and ξ_o is a constant dependent upon the gas. This will be the case so long as the fireball energy is trapped behind the shock and the pressure ratio behind and ahead of the shock is large (~10). As the shock expands outward, the temperature of the plasma behind it drops until the transparency temperature is reached. This is the temperature at which the plasma becomes transparent to the radiation that was previously in equilibrium with it. The radiation mean free path becomes large in comparison to the fireball dimensions. At this point the radiation "leaks" through the shock front and the temperature of the fireball falls more quickly than before. At this point, a free shock is launched with the temperature and pressure profiles decoupling as shown in Fig. 1-b. This shock then propagates to the first wall.

Computer Model

The phenomena described above are the result of a complex synergism between radiative processes and hydrodynamics. To more fully understand this complex process a computer model has been developed to include the essential features of the fireball dynamics. The computer code has been given the name FIRE. In the FIRE code, the plasma/gas motion is described in the one

fluid hydrodynamic approximation. The equation of motion is expressed in lagrangian coordinates as

$$\frac{\partial u}{\partial t} = -x^{\delta-1} \frac{\partial}{\partial m_o} (P+Q) \tag{1}$$

where m_o is the lagrangian variable defined as

$$dm_o = x^{\delta-1}\rho(x)dx. \tag{2}$$

The other quantities are the fluid velocity u, the total pressure P, the mass density ρ, and one spatial dimension x (δ=1 planar, δ=2 cylindrical, δ=3 spherical). The standard shock treatment using a Von Neumann artificial viscosity Q is used.[17] This spreads the shock front over about 3 finite difference zones while preserving the Heugoniot relations across the shock. This equation is solved for the fluid velocity using an explicit differencing technique which, for numerical stability, requires the satisfaction of the Courant condition[18]

$$\Delta t < \Delta x/C_s \tag{3}$$

where Δt is the time step, Δx is a finite difference zone width and C_s is the local sound speed. This limits the time step so that disturbances cannot propagate across a zone in less than one time step. The plasma is characterized by a local temperature $T_p(x,t)$. Thermal energy flow through the plasma includes electron thermal conduction and radiation transport. Radiation transport is treated by modelling the radiation field as a fluid with its own local temperature, $T_r(x,t)$.[19] This temperature can be different from the plasma temperature. Two coupled diffusion equations are then solved for the thermal transport in the plasma. These are

$$C_{vp} \frac{\partial T_p}{\partial t} = \frac{\partial}{\partial m_o} (x^{\delta-1} K_p \frac{\partial T_p}{dx}) - w_{pr}(T_p-T_r)-(P_p)_T \frac{\partial V}{\partial t} T_p \tag{4}$$

and

$$C_{vr} \frac{\partial T_r}{\partial t} = \frac{\partial}{\partial m_o} (x^{\delta-1} K_r \frac{\partial T_r}{\partial x}) + w_{pr}(T_p-T_r) - (P_r)_T \frac{\partial V}{\partial t} T_r. \tag{5}$$

where C_{vp} and C_{vr} are the specific heats at constant volume for the plasma and radiation, K_p[22] and K_r[19] are the thermal conductivities for the plasma and radiation, $(P_p)_T$ and $(P_r)_T$ are the temperature derivatives of the plasma and radiation pressures, and V is the plasma specific volume. The emission and absorption of radiation is treated by the coupling term $w_{pr}(T_r-T_p)$. For the calculation presented in this paper, the radiative transfer of energy is the most dominant effect. The two equations are solved simultaneously using a fully implicit finite difference technique.[21,22] Two "adjustments" must be added to the solution of these non-linear diffusion equations to insure physical relevance and numerical stability. First, the radiation diffusion equation is flux limited. The flux across a zone boundary is not allowed to exceed cE_r, which is the free streaming limit of radiation flux in a vacuum. This allows the diffusion model to be used in non-diffusive problems while continuing to provide physically plausible results. Second, upstream averaging is used to evaluate the radiation properties near the edge of the fireball. This allows radiation to flow from a hot zone where its heat capacity, $C_{vr} \sim T^3$, is high to a cold zone where its heat capacity is low without resorting to diminishingly small times to control accuracy. This also avoids bothersome numerical instabilities that result from this non-linear problem. The two-temperature approximation allows the radiation to come into equilibrium at whatever temperature that it wishes. This is shown schematically in Fig. 1a where the cold plasma is transparent to the radiation but the plasma at the edge of the fireball is not. Hence the radiation is the region between the fireball and the wall is in equilibrium with the hot plasma at the edge of the fireball while the plasma temperature between the fireball and the wall remains low. This is shown to be crucial to the results of fireball dynamics in noble gases. One temperature models[23], such as used in the CHART-D code, may not accurately treat

this phenomenon. Codes using multi-frequency radiation diffusion would of course offer a better model but these are much more expensive to use. The two temperature model used here is a good compromise.

A most important feature of this model is the equation of state and radiative property data. In fact, the behavior of these quantities in the non-linear coefficients of the hydrodynamics equations is the key to the results obtained in this paper. For the FIRE code, these data are stored in tabulated form as a function of density, plasma temperature, and radiation temperature. The tabulated quantities include: plasma specific internal energy $E(\rho,T_p)$, plasma average charge state $\bar{Z}(\rho,T_p)$, Planck averaged radiation mean free path $\ell_1(\rho,T_p,T_r)$, and Rosseland averaged radiation mean free path $\ell(\rho,T_p,T_r)$. These quantities are computed using a semi-classical model of the atom[24] using another computer code named MFP.[25] The Planck averaged mean free path is shown in Fig. 3 as a function of the plasma and radiation temperatures for a fixed argon plasma density.

For most of the calculations that follow the spherical cavity gas volume is divided into 50 spatial zones and 14,000 time steps are used to span 3-5 ms of physical time. These calculations require 3 ms/zone·cycle on a UNIVAC 1110 computer. This represents a modest cost for the computations.

Calculational Results

In the results that follow, it is assumed that the pellet X-ray and debris energy is stopped in the first 10 cm surrounding the pellet. This is the size of the initial fireball, at t = 0. The pellet mass is taken to be additional cavity gas mass (only one ion specie is allowed in the FIRE code) and is uniformly distributed in the 10 cm initial fireball. Equal mass zoning is used at the center of the gas volume (10 zones), near the initial

fireball, and also near the first wall (10 zones). This gives the most accurate treatment of the gas motion. In between (30 zones) there is a smooth variation in zone mass to avoid "numerical reflections" of lighter zones from heavier ones.

The details of a representative calculation are given in Table 1. The 30 MJ of yield that is deposited in the gas would correspond to a total yield of 100-150 MJ when the 14.1 MeV neutrons are included. This is a range of yield that is considered for light ion beam driven targets.[26,27] The general features of fireball dynamics that are described in the earlier section on phenomenology are numerically verified in this example. Figure 4 is a plot of the plasma temperature profiles in the plasma as a function of radius at different times during the shock propagation to the wall. Figure 5 is a similar plot of the pressure. Figure 6 is a plot of the heat flux and mechanical overpressure experienced at the first wall as a function of time and Fig. 7 is a plot of the Planck and Rosseland averaged radiation mean free paths as functions of the plasma and radiation temperatures when they are equal. Figure 7 shows that the argon plasma becomes transparent to its equilibrium radiation at a temperature of ~1 eV. Figure 4 shows that the fireball reaches this temperature at a time between 0.1 ms and 0.46 ms after the fireball creation and Fig. 6 indicates that this is when the first wall experiences the heat flux leaking from the fireball. Figures 4 and 5 show that the shock has separated from the fireball by 0.46 ms and propagates to the wall by itself. Figure 8 is an R-t plot of the gas motion. Each line in this plot follows the trajectory of a unit of mass as a function of time. The shock can be clearly seen as a bunching of the lines. The prediction of

Table 1

Input Parameters for FIRE Calculations

Cavity radius (m)	4	4
Gas type	Argon	Diatomic Ar
Gas pressure at 0°C (torr)	50	50
Gas number density (cm^{-3})	1.67×10^{18}	1.67×10^{18}
Gas mass density (g/cm^3)	1.114×10^{-4}	1.114×10^{-4}
Energy deposited in fireball (MJ)	30	30
Initial fireball radius (cm)	10	10
Initial fireball temperature (eV)	64	64
Initial fireball charge state	12	12
Maximum overpressure (atm)	1.5	2.75
Time of maximum overpressure (ms)	2.3	1.7
Energy radiated to wall (MJ)	7.5	0.15
Average heat flux* (kW/cm^2)	15	0.05
Pulse width* (μs)	110	1500

*The average heat flux is defined as the energy radiated to the first wall divided by the pulse width.

strong shock theory is also plotted on Fig. 8 and we see that the shock speed begins to deviate from strong shock theory early in time. The heat flux at the wall averaged over the pulse width is 15 kW/cm^2. This is unacceptably large for reactor applications. The resultant temperature rise in a 0.5 cm stainless steel wall is 317°C when the repetition rate is 10 Hz.

All of these results are attributable to the high transparency temperature of argon, Fig. 7. Air, for instance, has a transparency temperature of 0.2 eV. The high transparency of argon at temperatures below 1 eV is due to the monatomic nature of the molecule. Electronic transitions are the lowest transitions available to strongly absorb a photon. Hence, photons below about 16 eV are only weakly absorbed. This situation is much different for polyatomic molecules where the rotational and vibrational transitions are available to absorb low energy photons. Hence the transparency temperature of these gases is much lower. To demonstrate the importance of this point, the argon data used in the example calculation is modified so that the radiation mean free path path below 1.5 eV is limited to no greater than 50 cm. This gas we call "diatomic argon". The results of an identical calculation using this gas are also given in Table 1 and are displayed in Fig. 9. From Fig. 9 we see that the heat flux comes only after the pressure pulse has hit the first wall and the maximum heat flux is only 0.13 kW/cm^2. On the other hand, the overpressure is greater in this case because energy is never leaked from the fireball before the shock arrives at the wall. This comparison verifies the assertion that the high transparency of noble gases at low temperature leads to the premature release of the radiant energy in the fireball. Therefore, a strong distinction exists between the behavior of noble and non-noble gases in high pressure reactor cavities.

A variety of other calculations have been done to determine the effect of changing various important parameters. In Table 2 the tabulated results of calculations using different initial argon temperatures are given. In each case a 30 MJ fireball is started in the center 10 cm of the cavity. These different initial temperatures correspond to different mass flow rates of argon through the cavity for a system in cyclic steady state. The total radiant energy transferred to the first wall increases with increasing temperature. This is because the gas surrounding the fireball has an increasing amount of energy associated with it as its temperature increases. At a temperature of 1.0 eV for instance, there is more energy radiated to the first wall than is in the fireball. This is clearly a non-physical result. The point to be made here is that at a gas temperature between 0.7 and 1.0 eV (actually ~0.73 eV) the gas will radiate 30 MJ to the wall for every 30 MJ deposited into in at a repetition rate of 1 to 10 HZ. At this equilibrium point, no gas circulation through the cavity is needed to maintain cyclic steady-state operation at this temperature. To maintain cyclic steady state temperatures below 0.73 eV the gas must be circulated through an external heat exchanger. The mass flow rates are given for a 1 Hz repetition rate. The results of using xenon rather than argon as the cavity gas are given in Table 3. From this result, it is seen that for identical initial conditions, xenon gas allows a much lower amount of radiant heat to reach the first wall than argon gas. This occurs because the heat capacity of xenon is larger than that of argon so that 30 MJ of energy raises the gas to a lower temperature where a smaller percent of the energy is in radiation. With less radiant energy in the system, the heat fluxes should be lower. Also, the radiation mean free paths tend to be shorter for xenon than for argon. Even though there is less energy lost via radiation, the overpressure at the wall is no larger. The scaling of the results with target yield are also demonstrated

Table 2

Wall Overpressures and Radiant Heat Fluxes for Argon Cavity Gas at Different Temperatures

E_{in} = 30 MJ		$N_p = 1.67 \times 10^{18} cm^{-3}$			R_{wall} = 4 m
T_{pcav} (eV)	$P_{wall-max}$ (atm)	$P_{initial}$ (atm)	ΔP (atm)	E_{out} (MJ)	$\langle \underline{q} \rangle''_{pulse}$* ($kW/cm^2$)
0.05	1.3	.113	1.17	6.6	21.9
0.1	1.5	.275	1.23	7.5	15.0
0.5	2.5	1.33	1.17	14.7	24.5
0.7	2.75	1.98	.78	20.3	29.2
1.0	3.0	2.95	.05	148	52.6

*$\langle \underline{q} \rangle''_{pulse}$ is defined as the energy radiated to the first wall divided by the pulse width.

Table 3

Comparison of High Pressure Blast Waves

$N_p = 1.67 \times 10^{18} cm^{-3}$		$T_{pcav} = .1$ eV	
GAS SPECIES	ARGON	XENON	ARGON
E_{in} (MJ)	30	30	100
$P_{wall-max}$(atm)	1.5	1.5	4.26
P_{init} (atm)	.27	.26	.27
ΔP_{wall} (atm)	1.23	1.25	4.0
E_{out} (MJ)	7.5	3.5	17.1
$\langle \underline{q} \rangle''_{pulse} (\frac{kW}{cm^2})$ *	15	7.9	21.3
$\dot{m}$(gm/sec)	3.3×10^4	9.7×10^4	1.3×10^5

*$\langle \underline{q} \rangle''_{pulse}$ is defined as the energy radiated to the first wall divided by the pulse width.

in Table 3 where the 30 MJ shot in argon is compared to a 100 MJ shot. The 100 MJ shot would correspond to a total yield of 333-500 MJ. The average heat flux at the wall is not substantially greater for the 100 MJ fireball, but the maximum overpressure is nearly 3 times as large. This latter point indicates that although the absolute value of the overpressure is not well predicted by strong shock theory, the relative magnitudes scale linearly with the explosion energy as would be predicted by strong shock theory.

Conclusions of High Pressure Results

(1) The strong shock theory of Taylor[15] does not adequately treat the propagation of a fireball through typical light ion beam fusion reactor cavity gases. (2) The gas temperature and pressure profiles indicate that the shock wave separates from the fireball long before it reaches the wall of a 4m radius cavity. (3) Radiant heat fluxes measured at the first wall are large for argon gas at a pressure of 50 torr. These lead to high temperature transients in a stainless steel wall. (4) This large (~20 kW/cm^2) instantaneous heat flux is the result of an unusually high transparency temperature for noble gases. This allows the radiation to "leak"from the fireball while it is still very hot. (5) Diatomic gases may be better suited than noble gases for the cavity gas in light ion beam fusion reactors because they will not become as transparent and volumetrically radiate their energy to the first wall at high temperatures (~1 eV). (6) The heat flux experienced by the first wall for non-noble gases is very low although the maximum overpressure is greater. However, mechanical design studies[28] show that this mechanical overpressure can be easily accommodated using standard engineering design techniques, and stainless steel as the first wall material. (7) On the other hand, if a large heat flux can be tolerated, as in a "single shot facility" or a materials test facility with a low duty cycle, then noble gases offer the opportunity to reduce the overpressure created by the blast wave. (8) Heavier noble gases, such as xenon, have larger heat capacities and shorter radiation mean free paths and will be more effective than argon in protecting the first wall from large radiant heat fluxes.

(9) In general, gas protection of the first wall in LIB fusion reactors is substantiated by these results. The gas type and temperature can be tailored to meet a whole range of specific requirements.

III. Low Pressure Cavity Gas - Laser Fusion Applications

Phenomenology

The gas pressure in a laser fusion reactor cavity must satisfy two conflicting criteria. The gas density must be low enough to insure that the laser beams will not be steered from the target by laser induced gas breakdown. On the other hand, the gas density must be sufficiently high to stop the charged particle debris and X-rays from the exploding pellet before they reach the wall. Unfortunately, the first of these limits is unknown and the second depends on the output spectra of the target which is also not well established.

Theoretical estimates show that laser induced gas breakdown will occur at pressures of 0.1 to 1 torr for noble gases and laser intensities on the order of those required for laser fusion.[10-12] Noble gases are thought to be particularly important to laser fusion applications because they possess a high ionization potential compared to non-noble gases. This presumably increases the breakdown threshold intensity of the laser light. However, the theories of breakdown do not accurately describe the results of many experiments and the viability of cavity gases in laser fusion reactors still must be determined by experiment. For the purposes of this study we assume that pellets can be successfully irradiated in 0.25 torr of a noble gas such as Ar or Xe.

Calculations also indicate that 0.1-1.0 torr of xenon gas will stop the ion debris and X-rays for a representative pellet output spectra.[29] For this low pressure gas and the representative pellet spectra, the output energy will not be stopped in a small volume surrounding the pellet but will be distributed through the gas in some profile that may extend to the first wall.

The gas response to this deposited energy is very important because it must hold this energy and re-radiate it to the first wall in a long pulse (~msec). This is the key element of the gas protection scheme proposed in the SOLASE laser fusion reactor study.

Computer Model

The computer model used for these calculations is the same one described in Part II. We should note that the low pressure gas calculations extend this model to its limit of validity because much of the phenomena that are predicted are non-diffusive in nature. This means that the model is operating in the flux limited mode for much of the calculation. However, the physical plausibility of the results will be stressed where appropriate.

Computational Results

In the following calculations, equal radii zoning is used rather than equal mass zoning. This makes very little difference in these computations because there is almost no motion of the gas.

In Table 6 we present the results of a calculation for 0.25 torr of xenon in a 6 meter cavity with a deposited energy of 30 MJ. This energy is assumed to be uniformly deposited in a 1 meter sphere surrounding the pellet. These results might be considered to correspond to the SOLASE reactor cavity situation. The heat flux and overpressure experienced at the first wall are shown in Fig. 10. The average heat flux, computed as the energy radiated to the wall in the high intensity part of the pulse divided by the width of this pulse, is 40.2 kW/cm^2. This heat flux is much higher than the estimate

Table 6

Fireball Calculation of 1/4 torr of Xenon in a 6 meter Cavity

Cavity Radius	6 meter
Gas Type	Xe
Gas Pressure (0°C)	0.25 torr
Energy Deposited	30 MJ
Initial Fireball Radius	1 meter
Initial Fireball Temperature	23.5 eV
Initial Gas Temperature	0.1 eV
Maximum Overpressure	13.7 torr
Time of Maximum Overpressure	23 μs
Energy Radiated to First Wall*	10 MJ
Average Heat Flux**	40.2 kW/cm^2
Pulse Width**	55 μs

* The energy radiated to the wall is defined as the amount of energy radiated for instantaneous values of the heat flux greater than 10% of the maximum.

** The average heat flux is defined as the energy radiated to the first wall divided by the pulse width.

used in the SOLASE study and leads to a temperature rise in the first wall of 1740°C. However, the overpressure experienced at the wall is very low, 14 torr. This is lower than the design value in SOLASE.

The reason for this very large heat flux can be learned from studying the plasma and radiation temperature profiles in the xenon gas along with the radiation mean free path. A snapshot plot of these is given in Fig. 11 at a time of 0.65 μs. This low pressure calculation is significantly different in character than the high pressure ones discussed in Part III of this paper. In this low pressure case the radiation mean free path in the hot fireball is very long and the mean free path in the surrounding cold gas is very long. However, in the temperature gradient between these two, there is a region of plasma where the mean free path is short. This is at a radius of about 400 cm in the snapshot shown in Fig. 11. This opaque region of plasma prevents the radiation behind it from streaming to the first wall. Note that the radiation temperature in the fireball has nearly come into equilibrium with this plasma region at a temperature of 2 eV, while the plasma temperature in the fireball is still 5-10 eV. This decoupling of the temperatures points out the importance of the two temperature model used in these calculations. This situation continues until this opaque plasma region has propagated to the first wall, at 2.8 μs. At this time the first wall is almost instantaneously exposed to all of the hot plasma behind this barrier; the fireball volumetrically radiates to the first wall. This results in a very large instantaneous heat flux. The heat flux decays very quickly because the fireball is rapidly losing energy and its temperature is dropping. Thus in this example the cavity gas very

effectively holds the explosion energy until the thermal wave created by the energy deposition reaches the first wall. Then the energy is rapidly radiated to the first wall.

The rather special set of circumstances that lead to this result cast doubt on the general applicability of this behavior over the range of uncertainties associated with the fireball creation process. The initial conditions are of course determined by the pellet output spectra. This problem is studied parametrically by assuming that the pellet energy is deposited in spheres of radii 1 meter, 3 meters, and 5 meters surrounding the pellet. The results of all of these calculations are presented in Table 7 for a 30 MJ charged particle and X-ray yield and 0.25 torr of xenon in a 6 meter cavity. As the initial fireball radius becomes larger, the amount of energy radiated to the wall increases but the time over which this energy is radiated also increases substantially. Hence the average heat flux incident on the wall decreases with increasing fireball radius. However, this heat flux is still substantial and the gas displays the same characteristics in all three cases. It only holds the deposited energy for about 0.1 msec whereas the graphite wall designs require a re-radiation time of greater than 1.0 msec.

A comparison of three different yield energies (10 MJ, 30 MJ, 100 MJ) is given in Table 8. These would roughly correspond to total pellet yields of 33, 100 and 330 MJ. The average heat flux increases dramatically from a 30 MJ to 100 MJ yield whereas the increase is only a factor of two between 10 MJ and 30 MJ yields. This can be explained by noting that the gas temperature rapidly drops to about 0.5-1.0 eV in all cases once the fireball reaches the wall. The energy radiated to the wall is then the difference

Table 7

Comparison of 1, 3, and 5 m Fireballs for a 30 MJ Fireball in 1/4 Torr of Xenon

	Fireball Radius		
	1 m	3 m	5 m
Cavity Radius (m)	6	6	6
Gas Type	Xe	Xe	Xe
Gas Pressure (0°C) (torr)	0.25	0.25	0.25
Energy Deposited (MJ)	30	30	30
Initial Fireball Temperature (eV)	23.5	4.5	2.0
Initial Gas Temperature (eV)	0.1	0.1	0.1
Maximum Overpressure (torr)	13.7	15.2	18.2
Time of Maximum Overpressure (μs)	23	25	1000
Energy Radiated to First Wall* (MJ)	10	14.5	14.7
Average Heat Flux** (kW/cm^2)	40.2	25.6	18.5
Pulse Width** (μs)	55	125	175

*The energy radiated to the first wall is defined as the amount of energy radiated for instantaneous values of the heat flux greater than 10% of the maximum.

**The average heat flux is defined as the energy radiated to the first wall divided by the pulse width.

Table 8

Comparison of Different Yields for 0.25 Torr Xenon in a 6 m Cavity

	Energy Deposited (MJ)		
	10	30	100
Cavity Radius (m)	6	6	6
Gas Type	Xe	Xe	Xe
Gas Pressure (0°C) (torr)	0.25	0.25	0.25
Initial Fireball Radius (m)	1	1	1
Initial Fireball Temperature (eV)	14	23.5	35
Initial Gas Temperature (eV)	0.1	0.1	0.1
Maximum Overpressure (torr)	2.4×10^{-3}	13.7	83.6
Time of Maximum Overpressure (μs)	1000	23	1.8
Energy Radiated to First Wall* (MJ)	2.0	10	53
Average Heat Flux** (kW/cm^2)	20	40.2	532
Pulse Width** (μs)	22	55	22

*The energy radiated to the first wall is defined as the amount of energy radiated for instantaneous values of the heat flux greater than 10% of the maximum.

**The average heat flux is defined as the energy radiated to the first wall divided by the pulse width.

between the initial energy and the energy content of the gas at a temperature of 1 eV. With only 10 MJ initially in the gas, this difference is quite small. For a 30 MJ yield this difference is about 10-20 MJ and for 100 MJ this difference is 80-90 MJ. Hence the average heat flux scales roughly as the difference between the initial fireball energy and 10 MJ rather than just the initial fireball energy.

Such a scaling of the radiant heat flux with fireball energy should also be affected by the cavity radius. For a 6 m cavity radius the gas does not begin radiating to the first wall until the thermal wave reaches it. The results of varying the cavity radius are given in Table 9. These results indicate the fact that once the cavity radius is greater than 6 m the fireball becomes transparent before the thermal wave reaches the wall. This is similar to the results at high gas pressure. This effect is clearly demonstrated in Fig. 12 and Fig. 13. These are snapshot plots of the plasma and the radiation temperatures at different times. Note that at 12.8 μs and 406 μs the radiation temperature is uniform throughout the cavity, indicating that the transparency limit has been reached. This occurs at very nearly the same time that the thermal wave reaches 6 m in radius. Surprisingly, the 8 m and 12 m cavity heat flux results do not scale as R^{-2}. Even though the fireball becomes transparent before reaching the wall in each case, there is a difference in the rate of radiation to the wall. This is almost a factor of two faster in the 12 m cavity. Hence the heat flux on the 12 m cavity wall is not $(8/12)^2$ times less than in the 8 m cavity, but is only about 20% less.

In Table 10, we compare the response of 0.25 torr of Xe to Ar for a 30 MJ fireball. The overpressures in each case are negligible. The fundamental

Table 9

Comparison of Different Cavity Radii for a 30 MJ Fireball in 1/4 Torr of Xenon

	Cavity Radius		
	6 m	8 m	12 m
Gas Type	Xe	Xe	Xe
Gas Pressure (0°C) (torr)	0.25	0.25	0.25
Energy Deposited (MJ)	30	30	30
Initial Fireball Radius (m)	1	1	1
Initial Fireball Temperature (eV)	23.5	23.5	23.5
Initial Gas Temperature (eV)	0.1	0.1	0.1
Maximum Overpressure (torr)	13.7	4.2	1.4
Time of Maximum Overpressure (μs)	23	1000	1000
Energy Radiated to the First Wall*(MJ)	10	11.1	12.4
Average Heat Flux**(kW/cm^2)	40.2	13.8	11.4
Pulse Width** (μs)	55	100	60

*The energy radiated to the wall is defined as the amount of energy radiated for instantaneous values of the heat flux greater than 10% of the maximum.

**The average heat flux is defined as the energy radiated to the first wall divided by the pulse width.

Table 10

Comparison of the Response of Xenon and Argon to a 30 MJ Fireball

	Xe	Ar
Cavity Radius (m)	6	6
Gas Pressure (0°C) (torr)	0.25	0.25
Energy Deposited (MJ)	30	30
Initial Fireball Radius (m)	1	1
Initial Fireball Temperature (eV)	23.5	26
Initial Gas Temperature (eV)	0.1	0.1
Maximum Overpressure (torr)	13.7	16.0
Time of Maximum Overpressure (μs)	23	9.5
Energy Radiated to First Wall* (MJ)	10	11.9
Average Heat Flux**	40.2	105
Pulse Width**	55	25

* The energy radiated to the wall is defined as the amount of energy radiated for instantaneous values of the heat flux greater than 10% of the maximum.

** The average heat flux is defined as the energy radiated to the first wall divided by the pulse width.

dynamics of the fireball is the same for each gas, but the higher heat capacity of xenon allows it to hold the radiant energy better than argon. The average heat flux for argon, once the thermal wave reaches the wall, is about 2.5 times as large as for xenon. However, this makes little difference in the thermal response of the wall because the width of the heat pulse in both cases is quite small compared to the thermal time constant of most wall materials.

Finally, Table 11 is a comparison of the response of 0.25 torr of argon and 50 torr of argon in a 4 meter cavity for a 30 MJ fireball. As noted many times before, the fireball behavior is very different for these two gas pressures and this cavity radius. In the high pressure case, the overpressure at the wall is substantial and the heat flux is lower. In the low pressure case, the overpressure is negligible and the heat flux is very large. Solid first walls can be designed to handle the high overpressure/low heat flux conditions but the low overpressure/high heat flux conditions must be accommodated by increasing the cavity radius or placing a sacrificial material in front of the structural wall.

Table 11

Comparison of the Response of 0.25 torr Argon and 50 torr Argon to a 30 MJ Fireball in a 4 Meter Cavity

	1/4 torr	50 torr
Cavity Radius (m)	4	4
Gas Type	Ar	Ar
Energy Deposited (MJ)	30	30
Initial Fireball Radius (m)	1	0.10
Initial Fireball Temperature (eV)	26	64
Initial Gas Temperature (eV)	0.1	0.1
Maximum Overpressure (torr)	13.7	1140
Time of maximum overpressure (μs)	23	2000
Energy radiated to first wall* (MJ)	10	7.5
Average Heat Flux** (kW/cm^2)	40.2	15
Pulse Width** (μs)	55	248

*The energy radiated to the first wall is defined as the amount of energy radiated for instantaneous values of the heat flux greater than 10% of the maximum.

**The average heat flux is defined as the energy radiated to the wall divided by the pulse width.

Conclusions of Low Pressure Results

(1) For target yields of 100-1000 MJ, cavity radii of 6-12 m, initial fireball radii of 1-5 m and a gas pressure of 0.25 torr when measured at 0°C, inert cavity gases do not act as a thermal capacitor to hold up the energy of the microexplosion. Large instantaneous heat fluxes on the first wall lead to unacceptable temperature transients and thermal stress levels.

(2) The behavior of the fireball in the low pressure cavity is different from the high pressure case. The radiation mean free paths in the fireball and outside the fireball are long. The mean free paths in the temperature gradient between hot and cold regions are short. Consequently, the fireball does not drive a shock wave to the first wall, but instead a supersonic thermal wave propagates through a motionless gas. Once this opaque region of plasma in the temperature gradient reaches its transparency temperature, the fireball volumetrically radiates to the first wall. This combination of effects results in very high instantaneous heat fluxes but very low overpressures at the first wall.

(3) Xenon produces a first wall heat flux about 2.5 times less than argon under similar conditions.

(4) The heat flux at the first wall increases dramatically when the fireball energy is increased from 30 MJ to 100 MJ. This is because the heat flux is proportional to the difference between the fireball initial energy and about 10 MJ rather than just the absolute magnitude of the fireball energy.

(5) Increasing the radius of the initial fireball, determined by the pellet output spectra, reduces the heat flux on the first wall by increasing

the width of the radiation pulse. However, only a factor of three reduction is achieved between fireball radii of 1 and 3 meters.

(6) The heat flux incident on the first wall does not decrease as R^{-2} as the cavity radius increases. It decreases at a substantially slower rate because there is a thermal interaction between the gas near the first wall and the transparent radiating fireball. More energy is radiated from the fireball in the short X-ray burst when the wall is further from the fireball.

(7) In general, these results indicate that noble gases will not protect the first wall in laser fusion reactors from excessively large surface heat loads and the subsequently large thermal stresses or evaporation.

Implications of Results

The results presented in this paper indicate that noble gases, such as argon and xenon, may not be suitable for first wall protection in either light ion beam reactors or laser fusion reactors. In the case of light ion beams, calculations also indicate that non-noble gases, polyatomic gases, perform well in protecting the first wall. Hence, our general conclusion is that gas protection looks very attractive for light ion beam fusion since there is no restriction on the gas type and conventional first wall design appears to be acceptable.

However, for laser fusion applications it is thought that noble gases are particularly important because they have a higher resistance to laser induced gas breakdown than polyatomic gases. If noble gases are indeed required for laser fusion cavities, then first wall designs that can accommodate the high heat flux must be used. These will likely consist of a sacrificial

shield, or liner, in front of the structural first wall.[30] This concept has been studied previously for systems with no protection mechanism or only a partial protection such as magnetic fields which do not affect the pellet X-rays. Further analysis of the walls in gas protected laser fusion cavities should not rely upon the "thermal capacitor" effect of the gas which was incorrectly postulated.

Acknowledgement

This work was supported by Sandia Laboratory under Contract #DSG/06-9329.

References

1. J. Nuckolls, et al., "Laser Compression of Matter to Super High Densities: Thermonuclear (CTR) Applications", Nature 29, 139 (1972).

2. K. Brueckner and S. Jorna, "Laser-Driven Fusion", Rev. Mod. Phys. 46, 325 (1974).

3. G. R. Magelssen and G. A. Moses, "Pellet X-Ray Spectra for Laser Fusion Reactor Designs", Nucl. Fus. 19, 301 (1979).

4. R. W. Conn, "First Wall and Divertor Plate Material Selection in Fusion Reactors", J. Nucl. Mat. 76&77, 103 (1978).

5. G. Kulcinski, "First Wall Protection Schemes for ICF Reactors", J. Nucl. Mat. 85&86, 87 (1979).

6. L. A. Booth, "Central Station Power Generation by Laser Driven Fusion", LA-4858-MS, Los Alamos Scientific Laboratory (1972).

7. D. A. Freiwald, et al., "Laser Fusion Generating Stations Based on the Magnetic Protected Reactor Cavity", LA-UR-75-2035, Los Alamos Scientific Laboratory; also Trans. ANS 22, 68 (1975).

8. J. A. Maniscalco and W. R. Meier, "Liquid-Lithium Waterfall Inertial Confinement Fusion Reactor Concept,"Trans. ANS 26, 62 (1977).

9. M. Monsler, et al., "Electric Power from Laser Fusion: The HYLIFE Concept", Trans. ANS 30, 21 (1978).

10. R. W. Conn, et al., "SOLASE, A Laser Fusion Reactor Study", University of Wisconsin Fusion Engineering Program Report UWFDM-220, 1978.

11. G. A. Moses, et al., "The SOLASE Conceptual Laser Fusion Reactor Study", Proc. 3rd ANS Top. Meeting on Fusion Tech., p. 448.

12. S. I. Abdel-Khalik, "Engineering Problems of Laser Driven Fusion Reactors", Nucl. Tech. 43, 5 (1979).

13. D. L. Cook and M. A. Sweeney, "Design of Compact Particle Beam Driven Inertial Confinement Fusion Reactors", Proc. 3rd ANS Top. Meeting on Fusion Tech., p. 1178.

14. G. Yonas, "Fusion Power with Particle Beams", Sci. Am. 239, 50 (Nov. 1978).

15. G. Taylor, Proc. R. Soc. A201, 159 (1950).

16. V. Zeldovich and Y. Raizer, Physics of Shock Waves and High Temperature Hydrodynamic Phenomena, Academic Press (New York, 1966), Vol. I and II.

17. J. Von Neumann and R. Richtmyer, "A Method for the Numerical Calculation of Hydrodynamic Shocks", J. Appl. Phys. 21, 232 (1950).

References (cont.)

18. R. Richtmyer and K. Morton, Difference Methods for Initial Value Problems, Wiley (New York, 1967, 3nd Ed.), p. 323.

19. G. Fraley, et al., "Thermonuclear Burn Characteristics of Compressed Deuterium-Tritium Microspheres", Phys. Fld. 17, 474 (1974). (Appendix B).

20. L. Spitzer, "The Physics of Fully Ionized Gases", Interscience Publishers, (New York, 1962).

21. G. A. Moses, "PHD-I, A Plasma Hydrodynamics Computer Code", University of Wisconsin Fusion Engineering Program Report UWFDM-160, 1976.

22. R. Kidder and W. Barnes, "WAZER - A One-Dimensional, Two Temperature Hydrodynamic Code", Lawrence Livermore Laboratory Report UCRL-50583.

23. S. L. Thompson, "Improvements in the CHART-D Energy Flow Hydrodynamic Code V: 1972/73 Modifications", SLA-73-0477, Sandia Laboratories (1973).

24. Ref. 16, Chapter V.

25. R. R. Peterson and G. A. Moses, "MFP-A Calculation of Radiation Mean Free Paths, Ionization and Internal Energies in Noble Gases", University of Wisconsin Fusion Engineering Program Report UWFDM-307 (1979). (Submitted for publication to Computer Physics Communications.)

26. D. L. Cook, private communication.

27. R. Bangerter and D. Meeker, "Ion Beam Inertial Fusion Target Designs", Presented at Faculty Workshop on ICF Fusion, Argonne National Laboratory, June 5-9, 1978.

28. E. Lovell and R. Engelstad, "First Wall Mechanical Design for Light Ion Beam Fusion Reactors", University of Wisconsin Fusion Engineering Program Report UWFDM-322, Nov. 1979. (Submitted for publication to Nuclear Technology.)

29. T. O. Hunter and G. L. Kulcinski, "Description of the Reponse of Material to Pulsed Thermonuclear Radiation - Effect of Gases on Modification of Pellet Debris Spectra and First Wall Response", University of Wisconsin Fusion Engineering Report UWFDM-232, April 1978.

30. R. W. Conn, et al., "Studies of the Technological Problems of Laser Driven Fusion Reactors, The Pre-SOLASE Design", University of Wisconsin Fusion Engineering Program Report UWFDM-190, December 1976.

Figure Captions

Fig. 1 - Schematic history of blast wave. (a) Initially, radiation mean free paths ℓ are short at the shock front; fireball remains trapped behind the shock. (b) Fireball expands; temperature drops below $T_{transparent}$; ℓ becomes long at the shock front; radiation leaks to the first wall. (c) Temperature, lowered because of radiant heat loss, is so low that radiant heat transfer ceases and the fireball remains fixed in the gas while the shock hits the first wall.

Fig. 2 - Equilibrium gas and radiation specific energies for argon at $N = 1.67 \times 10^{18} cm^{-3}$ and $6.0 \times 10^{17} cm^{-3}$.

Fig. 3 - Planck mean free path in argon at $N = 2.7 \times 10^{19} cm^{-3}$.

Fig. 4 - Gas temperature profiles at various times for a 30 MJ explosion in $1.67 \times 10^{18} cm^{-3}$, 0.1 eV argon gas.

Fig. 5 - Gas pressure profiles at various times for a 30 MJ explosion in $1.67 \times 10^{18} cm^{-3}$, 0.1 eV argon gas.

Fig. 6 - Pressure and heat flux at a 4 meter radius first wall. A 30 MJ explosion sends a blast wave through $1.67 \times 10^{18} cm^{-3}$, 0.1 eV argon gas.

Fig. 7 - Rosseland and Planck mean free paths for radiation in $1.67 \times 10^{18} cm^{-3}$ argon. The radiation is assumed to be in equilibrium with the gas so that $T_r = T_p = T$.

Fig. 8 - Propagation of 30 MJ of energy through a $1.67 \times 10^{18} cm^{-3}$, 0.1 eV argon gas. The positions of the boundaries of 50 Lagrangian zones are plotted against time as is the position of a shock front predicted by strong shock theory.

Fig. 9 - Pressure and heat flux at a 4 meter radius first wall. A 30 MJ blast wave propagates through 1.67×10^{-18}, 0.1 eV "diatomic argon" gas. The radiation mean free paths are those of argon except when $T_r < 1.5$ eV, where they are limited to 50 cm.

Fig. 10 - Pressure and heat flux at a 6 meter first wall. A 30 MJ blast wave propagates through $8.88 \times 10^{15} cm^{-3}$, 0.1 eV xenon gas.

Fig. 11 - Gas temperature (solid line), radiation temperature (- -) and Planck mean free path (- . -) profiles at t = 0.65 μsec for a 30 MJ blast wave propagating through $8.88 \times 10^{15} cm^{-3}$, 0.1 eV xenon gas.

Fig. 12 - Gas temperature profiles at t = 12.8 μsec at t = 406 μsec for a 30 MJ explosion in $8.88 \times 10^{15} cm^{-3}$, 0.1 eV xenon gas.

Fig. 13 - Radiation temperature profiles at t = 12.8 μsec and t = 406 μsec for a 30 MJ explosion in $8.88 \times 10^{15} cm^{-3}$, 0.1 eV xenon gas.

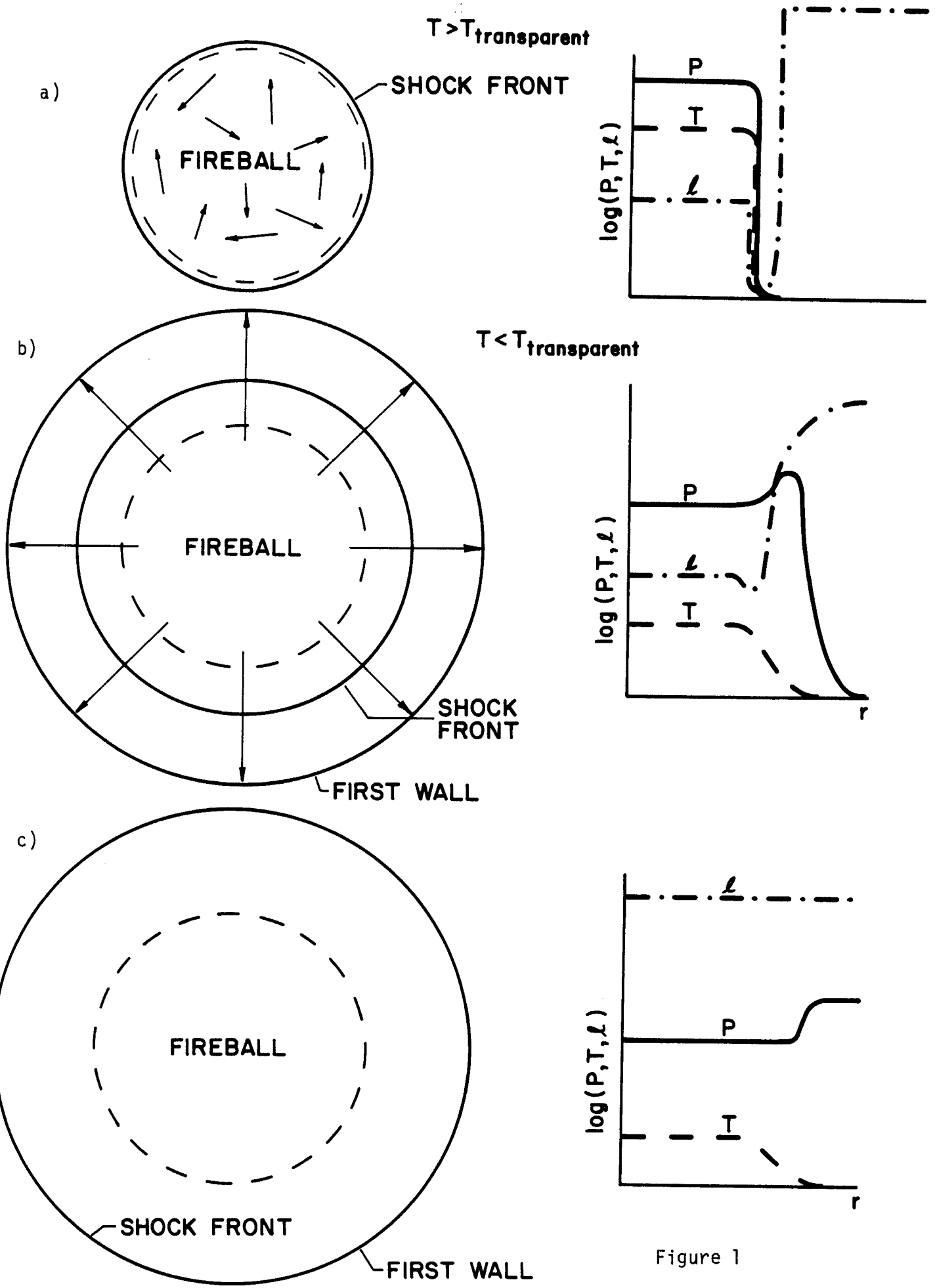
a)
FIREBALL
SHOCK FRONT
T>T transparent
P
T
ℓ
log(P,T,ℓ)
b)
FIREBALL
SHOCK FRONT
FIRST WALL
T<T transparent
P
ℓ
T
log (P,T,ℓ)
r
c)
FIREBALL
SHOCK FRONT
FIRST WALL
ℓ
P
T
log(P,T,ℓ)
r

Figure 1

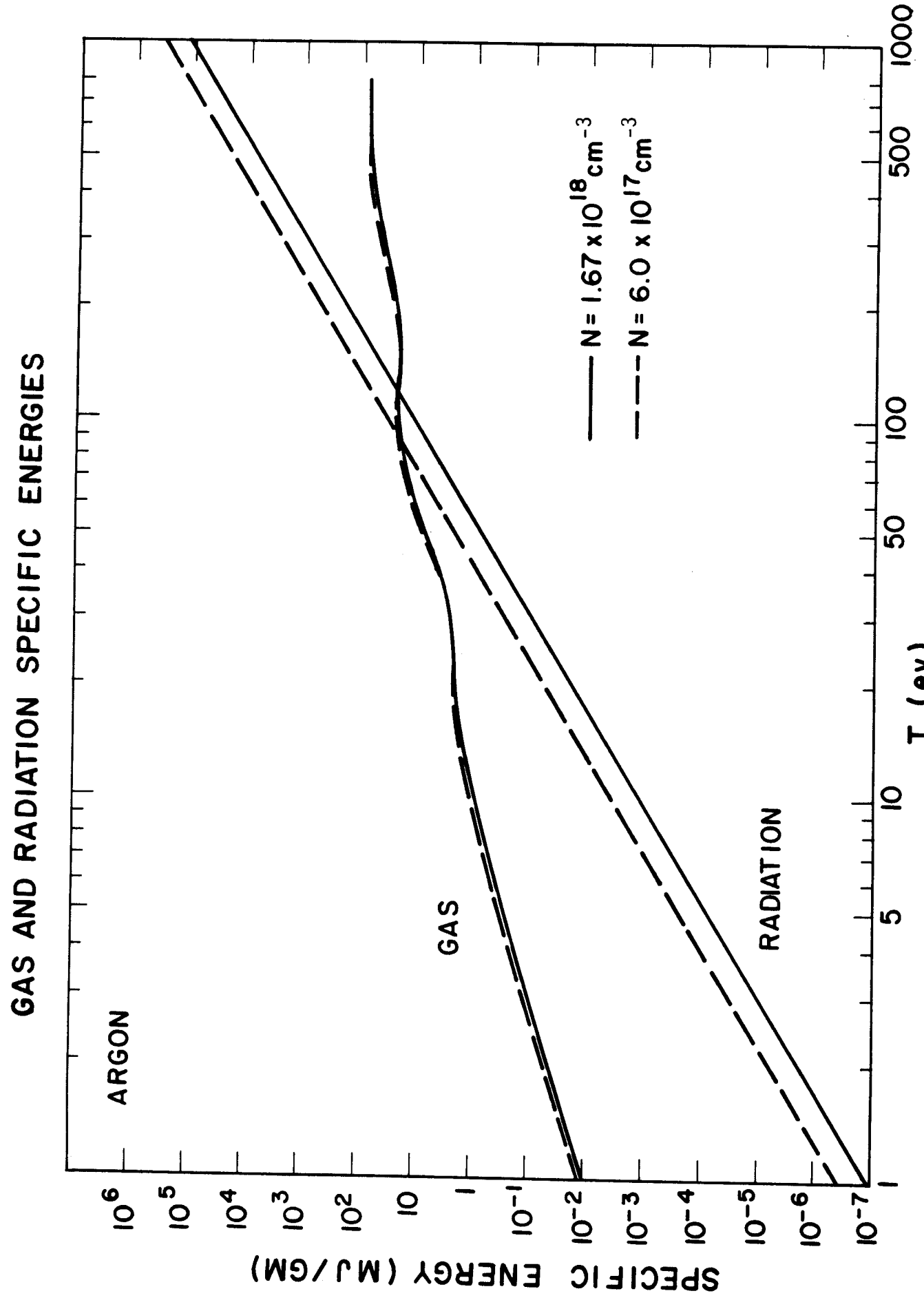
GAS AND RADIATION SPECIFIC ENERGIES
ARGON
GAS
RADIATION
N= 1.67 x 10^18 cm^-3
N= 6.0 x 10^17 cm^-3
SPECIFIC ENERGY (MJ/GM)
T (ev)
10^6
10^5
10^4
10^3
10^2
10
1
10^-1
10^-2
10^-3
10^-4
10^-5
10^-6
10^-7
1
5
10
50
100
500
1000

Figure 2

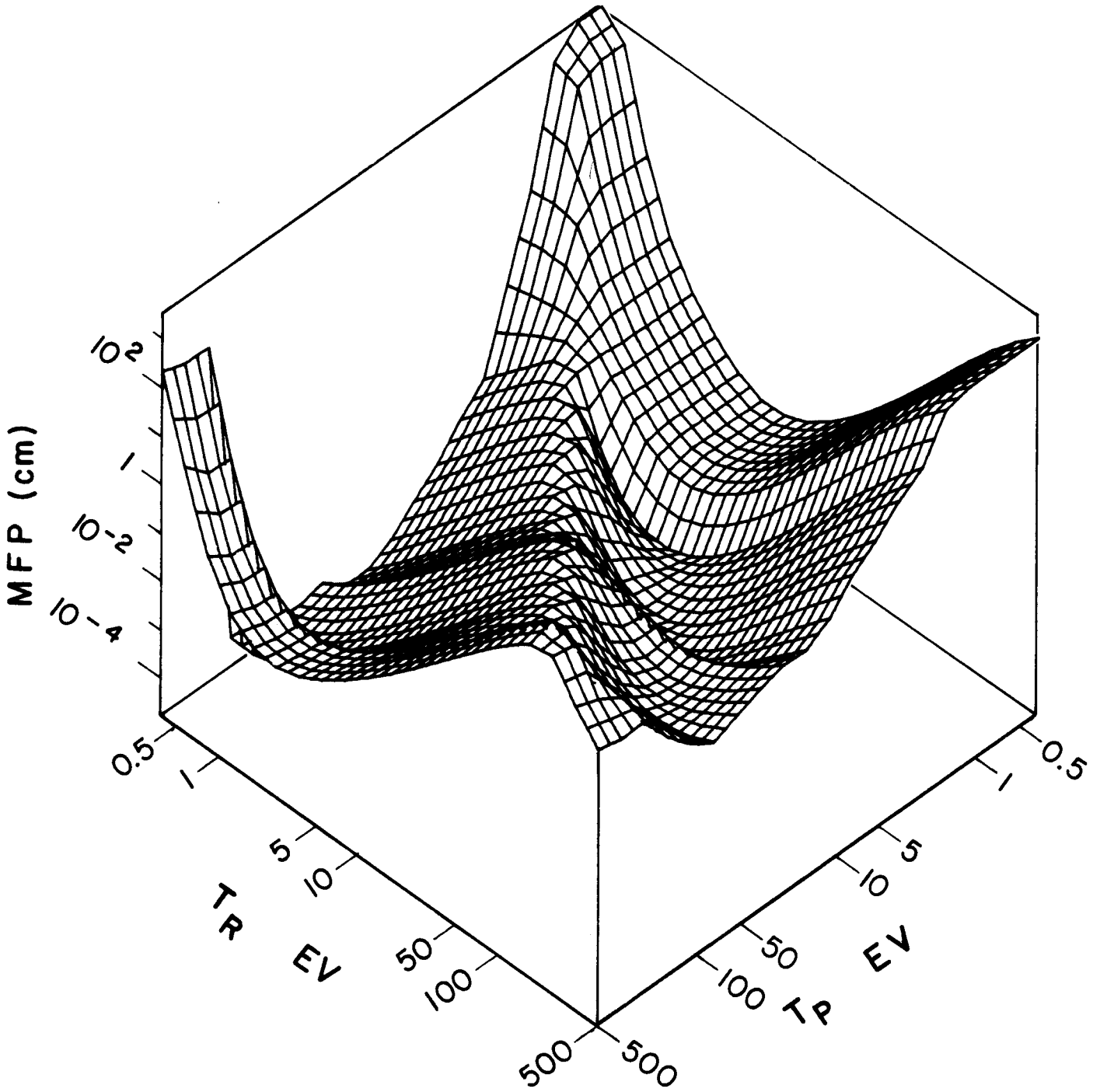

PLANCK MFP
ARGON DENSITY 2.7×10^{19} cm^{-3}

Figure 3

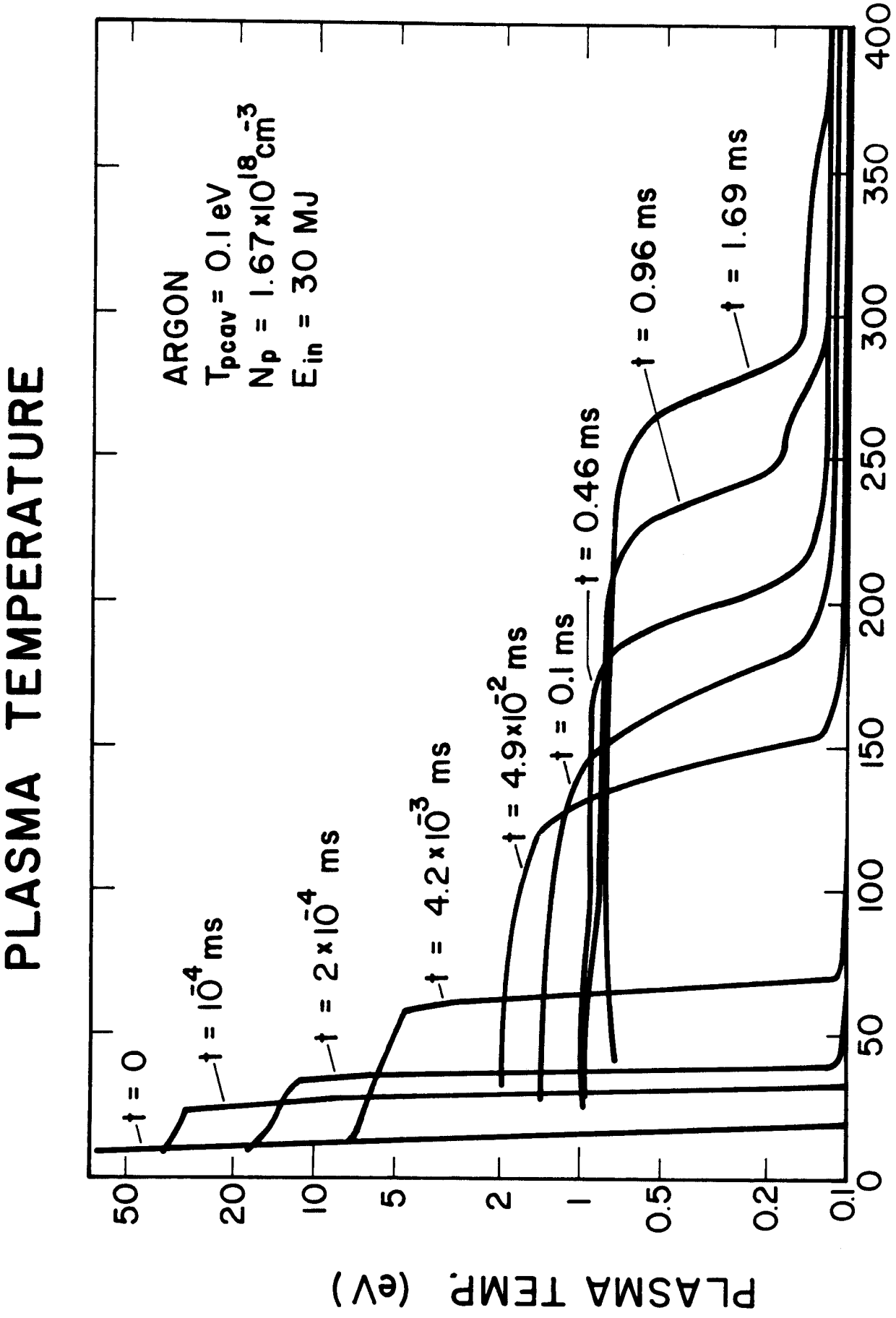
PLASMA TEMPERATURE
ARGON
T_{pcav} = 0.1 eV
N_p = 1.67x10^{18}cm^{-3}
E_{in} = 30 MJ
t = 0
t = 10^{-4} ms
t = 2x10^{-4} ms
t = 4.2x10^{-3} ms
t = 4.9x10^{-2} ms
t = 0.1 ms
t = 0.46 ms
t = 0.96 ms
t = 1.69 ms
PLASMA TEMP. (eV)
50
20
10
5
2
1
0.5
0.2
0.1
0
50
100
150
200
250
300
350
400
RADIUS (cm)

Figure 4

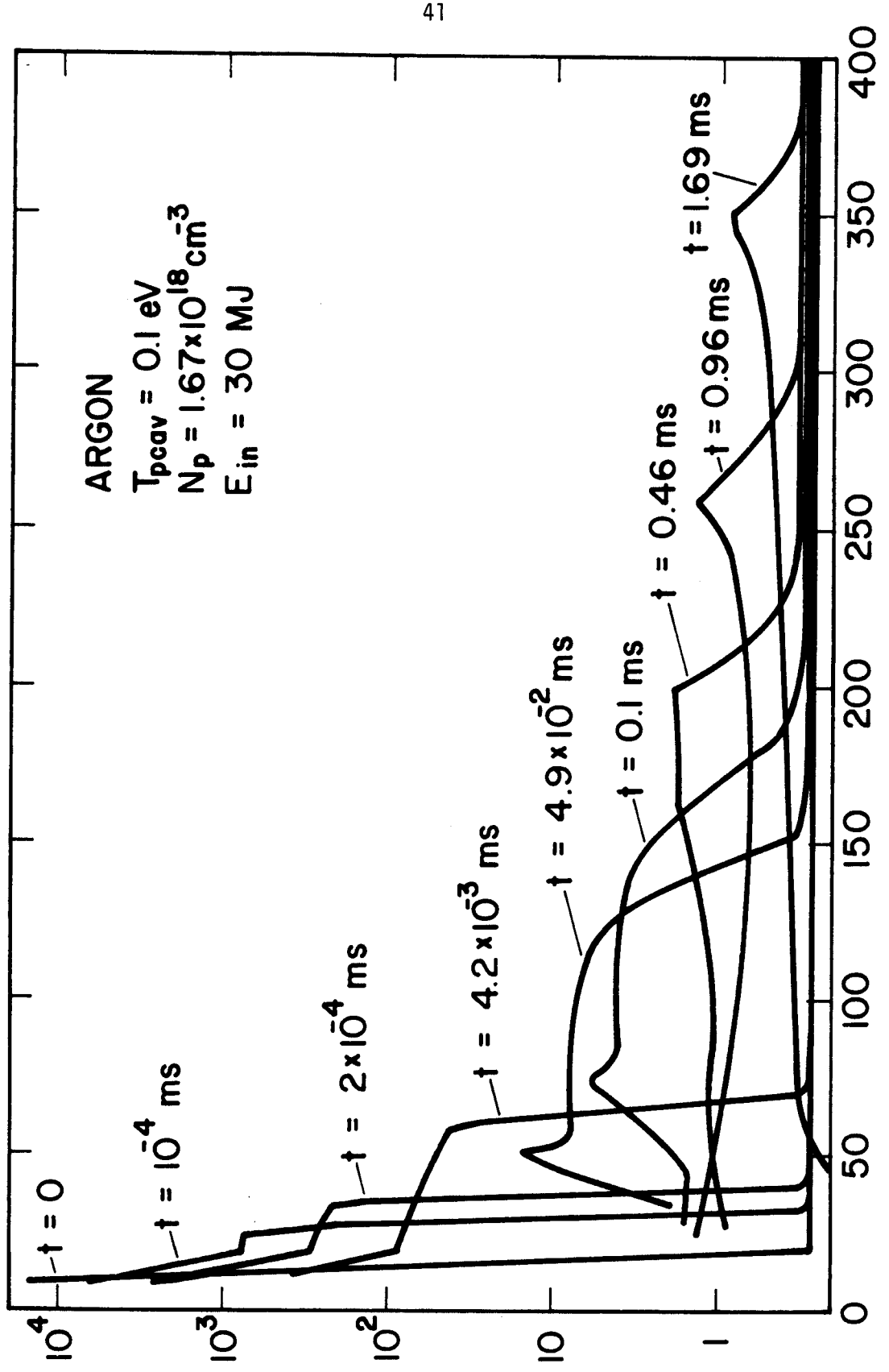
PLASMA PRESSURE
ARGON
T_{pcav} = 0.1 eV
$N_p = 1.67 \times 10^{18} cm^{-3}$
E_{in} = 30 MJ
t = 0
$t = 10^{-4}$ ms
$t = 2 \times 10^{-4}$ ms
$t = 4.2 \times 10^{-3}$ ms
$t = 4.9 \times 10^{-2}$ ms
t = 0.1 ms
t = 0.46 ms
t = 0.96 ms
t = 1.69 ms
PLASMA PRESS. (atm)
10^4
10^3
10^2
10
1
0
50
100
150
200
250
300
350
400
RADIUS (cm)

Figure 5

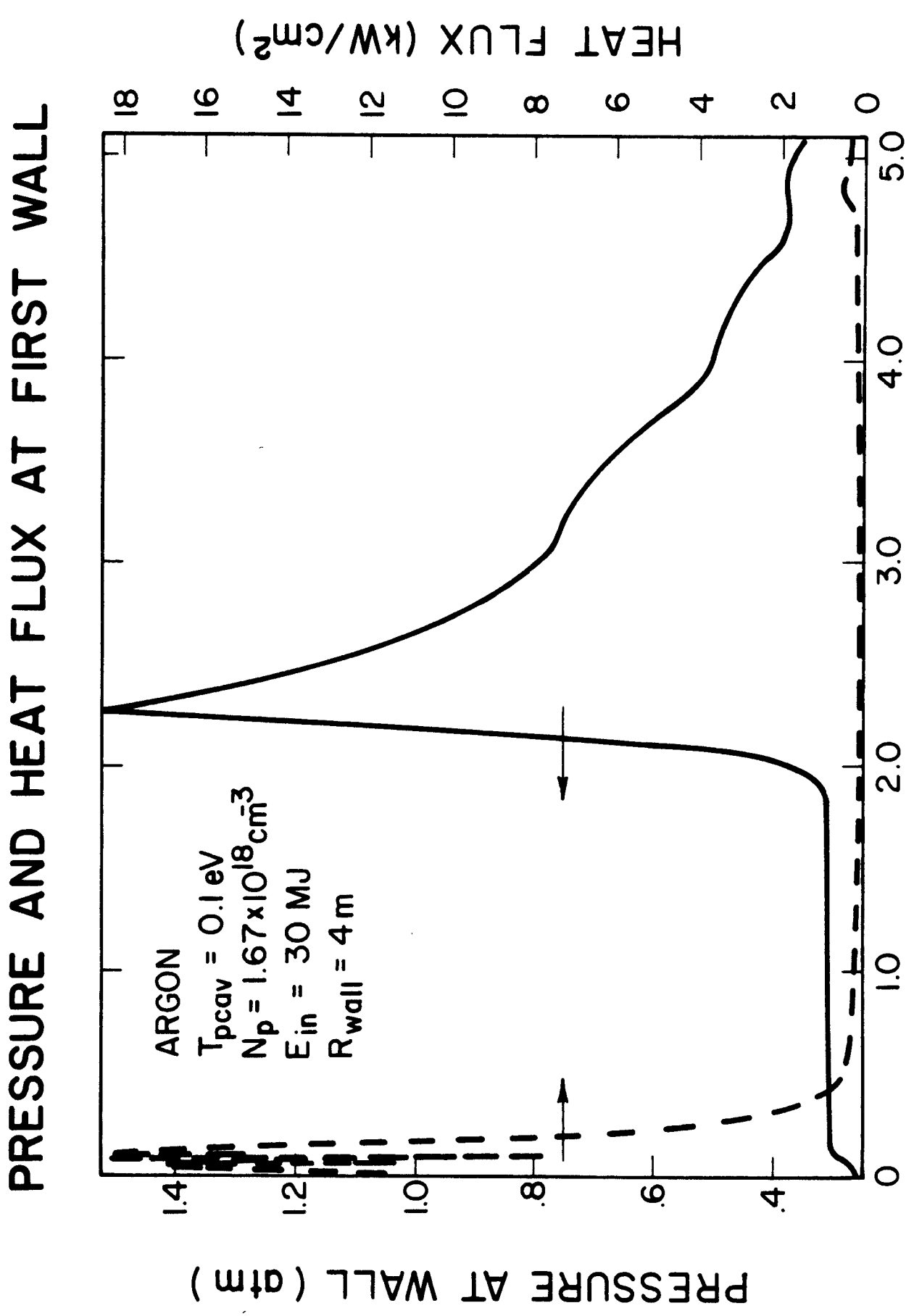
PRESSURE AND HEAT FLUX AT FIRST WALL
ARGON
T_{pcav} = 0.1 eV
N_p = 1.67x10^{18}cm^{-3}
E_{in} = 30 MJ
R_{wall} = 4 m
PRESSURE AT WALL (atm)
HEAT FLUX (kW/cm^2)
TIME (msec)
0
1.0
2.0
3.0
4.0
5.0
.4
.6
.8
1.0
1.2
1.4
0
2
4
6
8
10
12
14
16
18

Figure 6

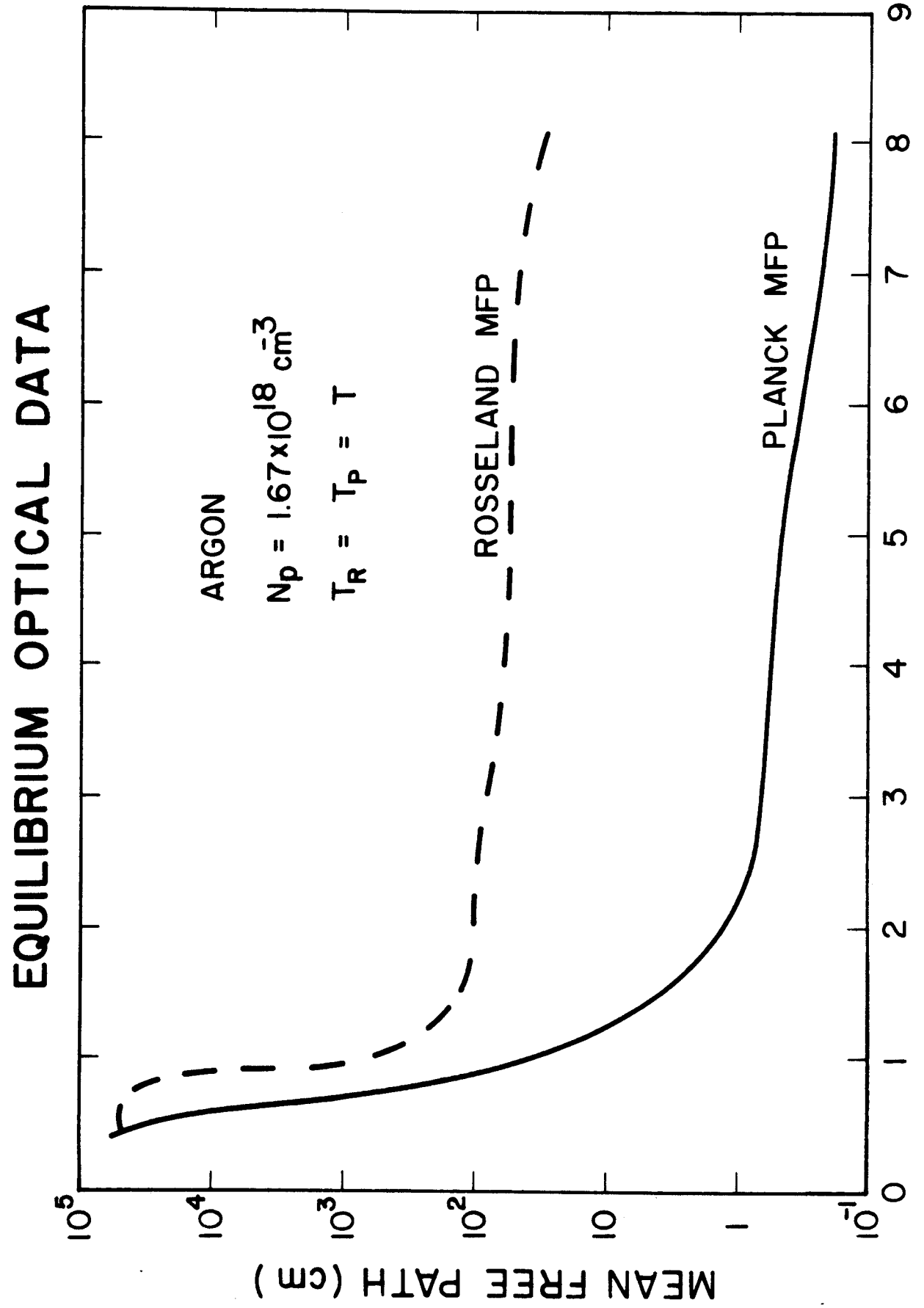
EQUILIBRIUM OPTICAL DATA
ARGON
$N_p = 1.67 \times 10^{18}\ cm^{-3}$
$T_R = T_P = T$
ROSSELAND MFP
PLANCK MFP
MEAN FREE PATH (cm)
10^5
10^4
10^3
10^2
10
1
10^{-1}
0
1
2
3
4
5
6
7
8
9
TEMPERATURE T (eV)

Figure 7

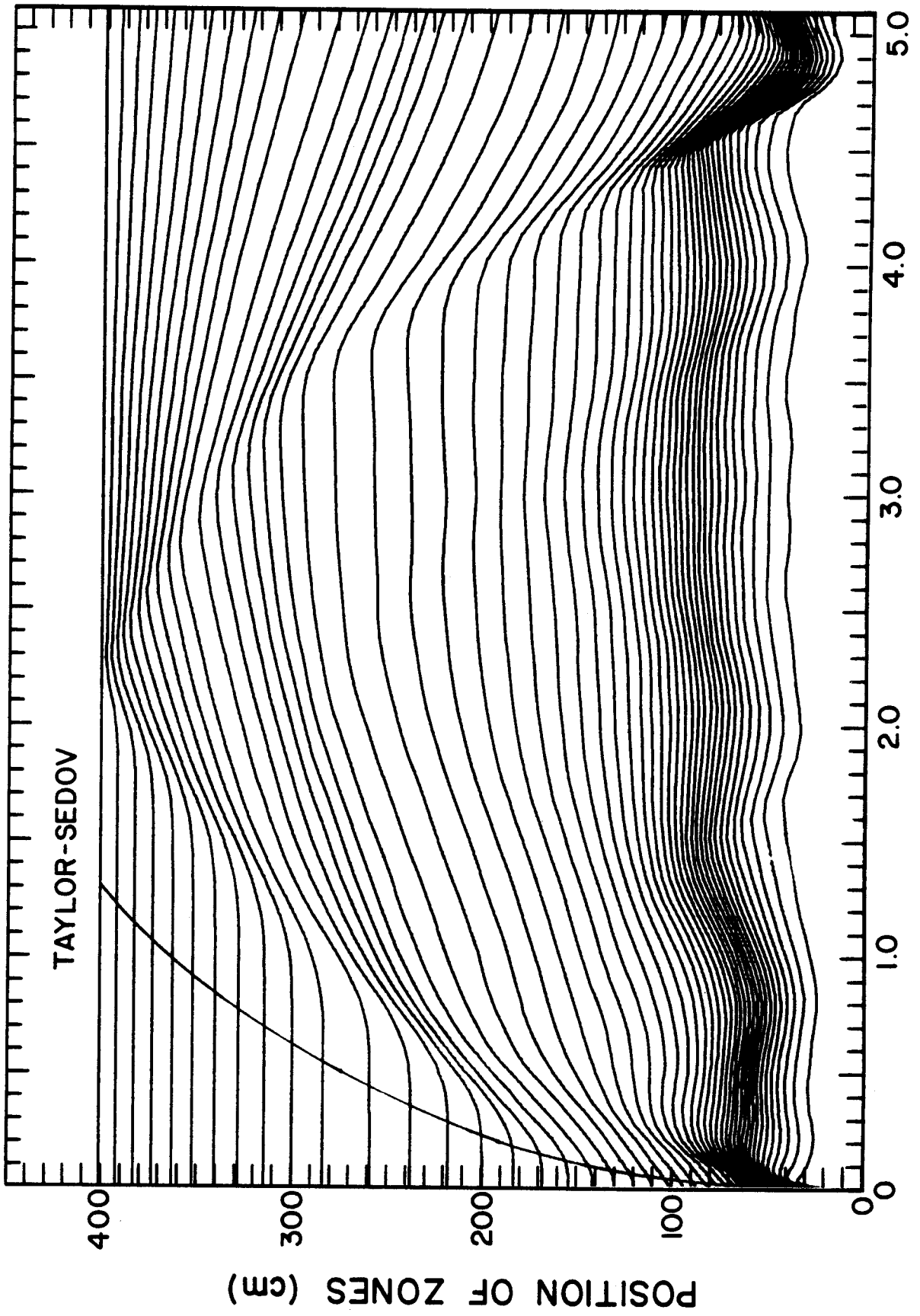
SHOCK PROPAGATION IN ARGON
T_{pcav} = 0.1 eV , N_p = 1.67x10^{18}cm^{-3} , E_{in} = 30 MJ
TAYLOR-SEDOV
POSITION OF ZONES (cm)
400
300
200
100
0
0
1.0
2.0
3.0
4.0
5.0
TIME (msec)

Figure 8

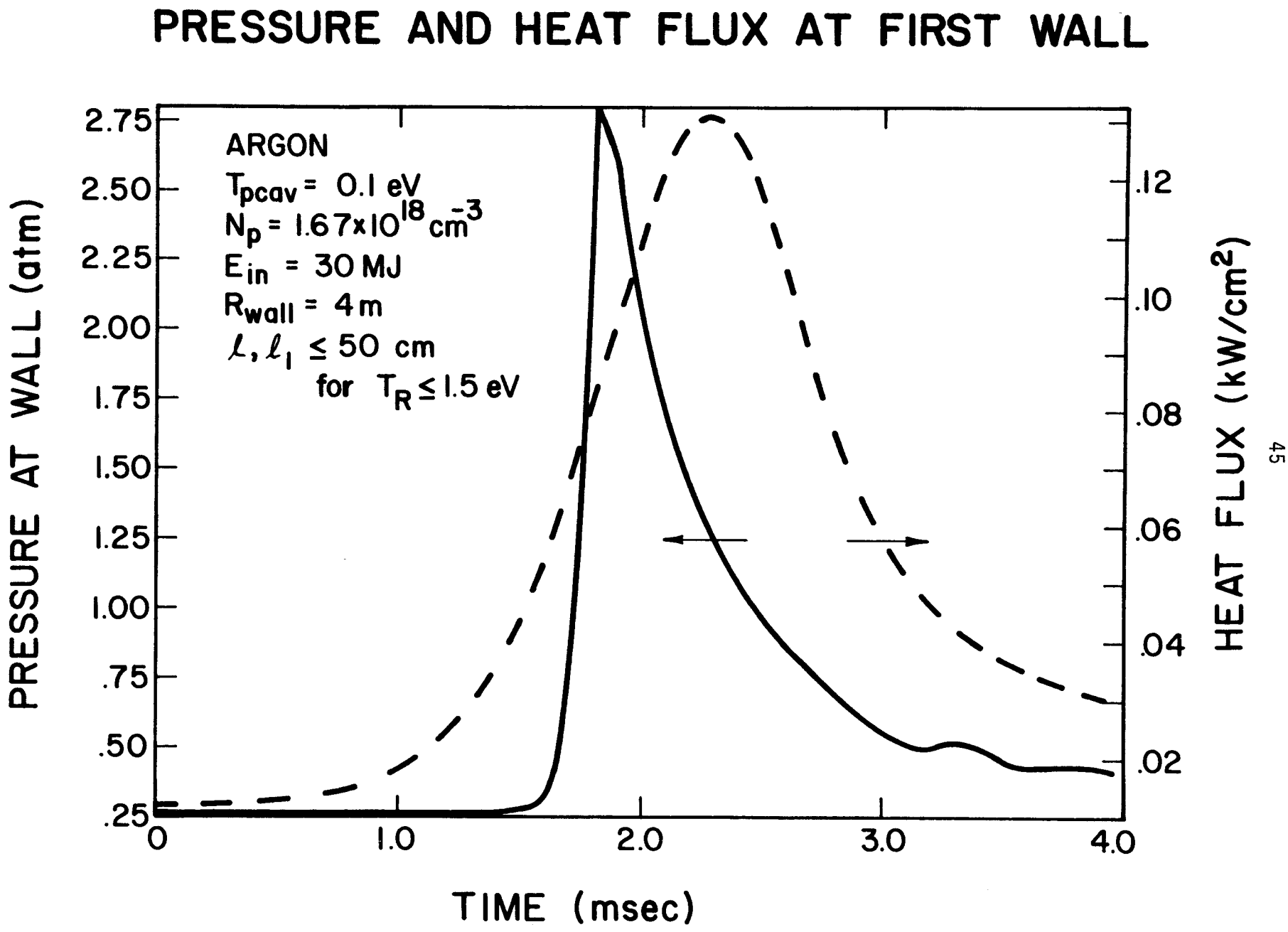
PRESSURE AND HEAT FLUX AT FIRST WALL
ARGON
T_{pcav} = 0.1 eV
$N_p = 1.67 \times 10^{18}$ cm^{-3}
E_{in} = 30 MJ
R_{wall} = 4 m
$\ell, \ell_1 \leq 50$ cm
for $T_R \leq 1.5$ eV
PRESSURE AT WALL (atm)
HEAT FLUX (kW/cm^2)
TIME (msec)
2.75
2.50
2.25
2.00
1.75
1.50
1.25
1.00
.75
.50
.25
.12
.10
.08
.06
.04
.02
0
1.0
2.0
3.0
4.0

Figure 9

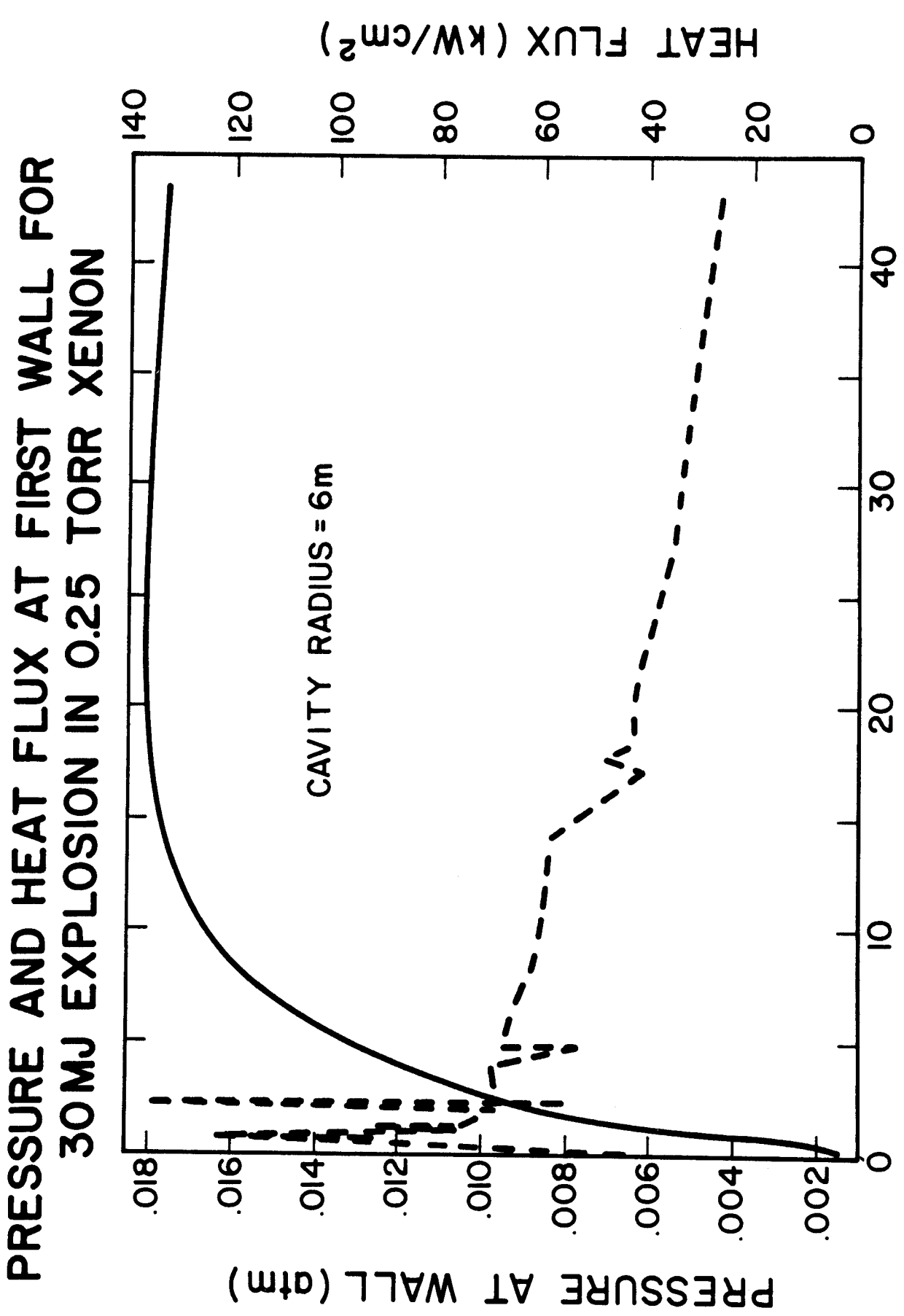
PRESSURE AND HEAT FLUX AT FIRST WALL FOR
30 MJ EXPLOSION IN 0.25 TORR XENON
CAVITY RADIUS = 6m
PRESSURE AT WALL (atm)
HEAT FLUX (kW/cm²)
TIME (μsec)
.018
.016
.014
.012
.010
.008
.006
.004
.002
140
120
100
80
60
40
20
0
0
10
20
30
40

Figure 10

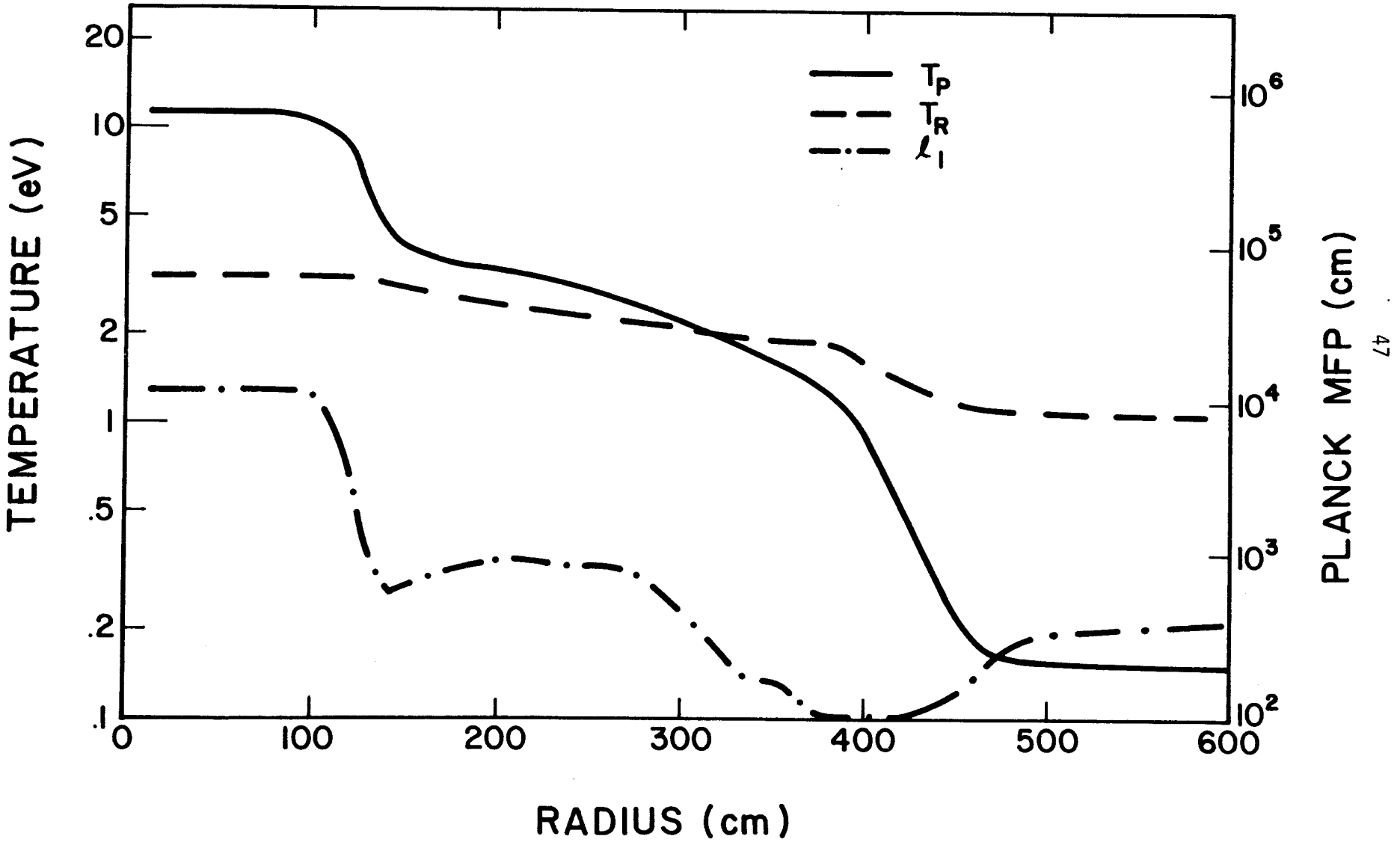
PLASMA TEMPERATURE, RADIATION TEMPERATURE, AND PLANCK MFP AT 0.65 μs FOR 30 MJ EXPLOSION IN 0.25 TORR OF XENON
TEMPERATURE (eV)
20
10
5
2
1
.5
.2
.1
T_P
T_R
ℓ_1
10^6
10^5
10^4
10^3
10^2
PLANCK MFP (cm)
0
100
200
300
400
500
600
RADIUS (cm)

Figure 11

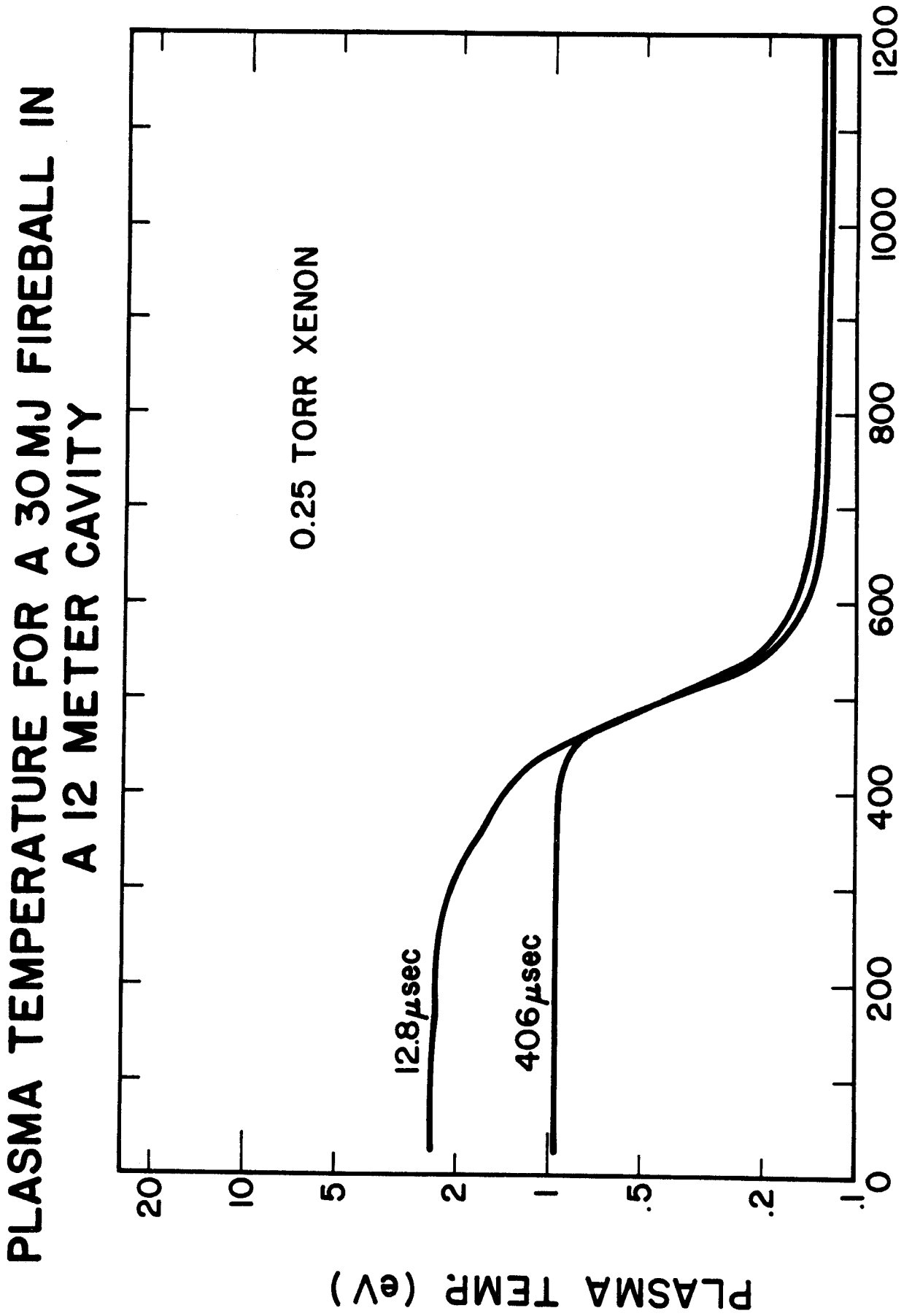
PLASMA TEMPERATURE FOR A 30 MJ FIREBALL IN A 12 METER CAVITY
0.25 TORR XENON
12.8μsec
406μsec
PLASMA TEMP. (eV)
20
10
5
2
1
.5
.2
.1
0
200
400
600
800
1000
1200
RADIUS (cm)

Figure 12

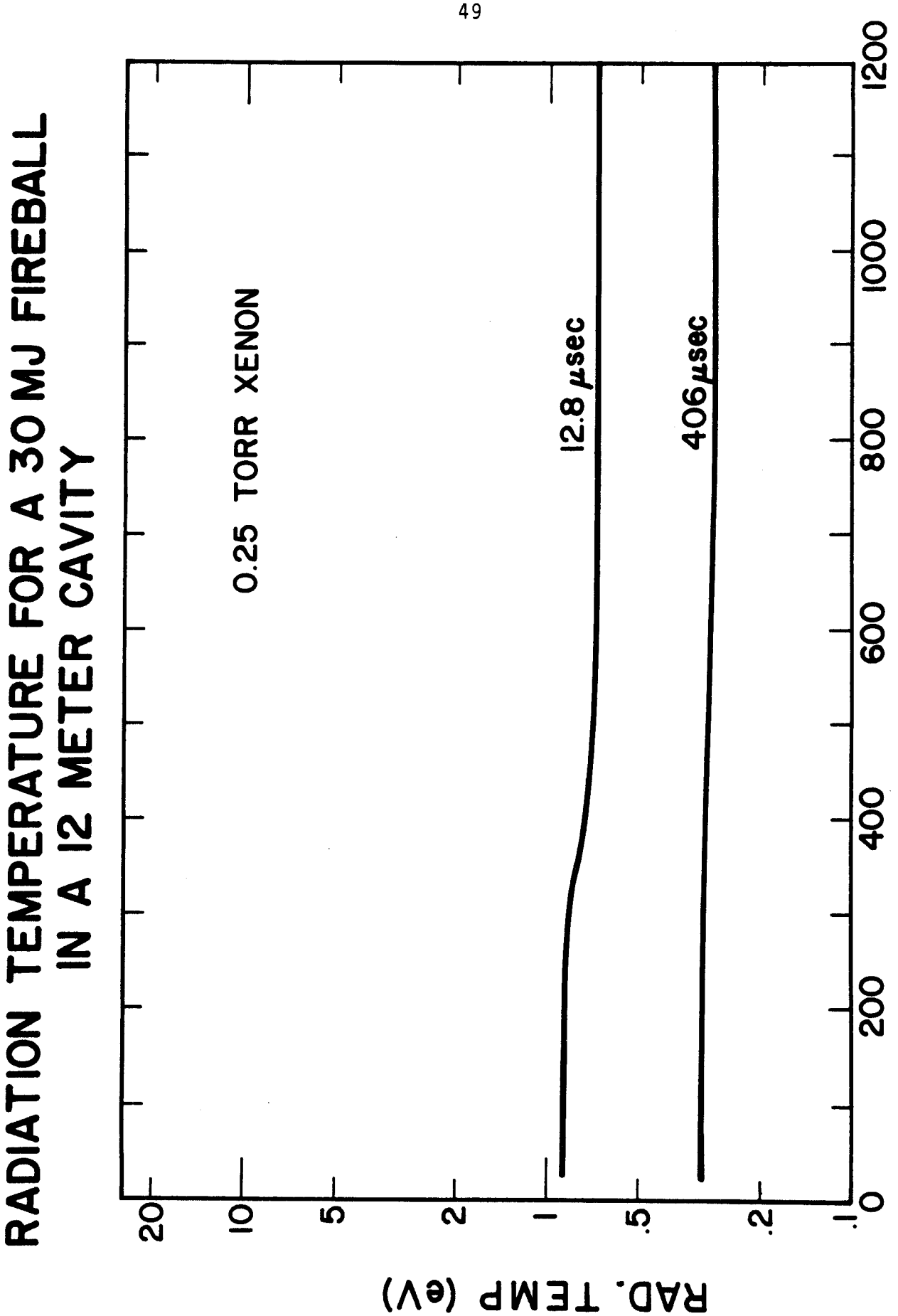
RADIATION TEMPERATURE FOR A 30 MJ FIREBALL
IN A 12 METER CAVITY
0.25 TORR XENON
12.8 μsec
406 μsec
RAD. TEMP (eV)
20
10
5
2
1
.5
.2
.1
0
200
400
600
800
1000
1200
RADIUS (cm)

Figure 13